RESEARCH ARTICLE

Probing the Efficiency of PPMG-Based Composite Electrolytes for Applications of Proton Exchange Membrane Fuel Cell

Shakeel Ahmed[1] · Faizah Altaf[2] · Safyan Akram Khan[2] · Sumaira Manzoor[2] · Aziz Ahmad[2] · Muhammad Mansha[2] · Shahid Ali[2] · Ata-ur-Rehman[2] · Karl Jacob[3]

Abstract
PPMG-based composite electrolytes were fabricated via the solution method using the polyvinyl alcohol and polyvinylpyrrolidone blend reinforced with various contents of sulfonated inorganic filler. Sulfuric acid was employed as the sulfonating agent to functionalize the external surface of the inorganic filler, i.e., graphene oxide. The proton conductivities of the newly prepared proton exchange membranes (PEMs) were increased by increasing the temperature and content of sulfonated graphene oxide (SGO), i.e., ranging from 0.025 S/cm to 0.060 S/cm. The induction of the optimum level of SGO is determined to be an excellent route to enhance ionic conductivity. The single-cell performance test was conducted by sandwiching the newly prepared PEMs between an anode (0.2 mg/cm^2 Pt/Ru) and a cathode (0.2 mg/cm^2 Pt) to prepare membrane electrode assemblies, followed by hot pressing under a pressure of approximately 100 kg/cm^2 at 60 °C for 5–10 min. The highest power densities achieved with PPMG PEMs were 14.9 and 35.60 mW/cm^2 at 25 °C and 70 °C, respectively, at ambient pressure with 100% relative humidity. Results showed that the newly prepared PEMs exhibit good electrochemical performance. The results indicated that the prepared composite membrane with 6 wt% filler can be used as an alternative membrane for applications of high-performance proton exchange membrane fuel cell.

Keywords Proton exchange membrane fuel cell · Sulfonated graphene oxide · Polyvinylpyrrolidone · Solution casting · Membrane electrode assembly · Fuel cell performance

Introduction

Future energy resources should be not only energy efficient but also environmentally friendly to minimize the fast depletion of fossil fuels and mitigate their detrimental effects on the environment [1]. To address this issue, many emerging technologies have been employed to increase the efficiencies of energy conversion devices, such as supercapacitors, batteries, and fuel cells (FCs) [2, 3], depending on their applications. Among FC selections, proton exchange membrane fuel cells (PEMFCs) are more promising in the field of clean energy conversion devices [4]. A single PEMFC is composed of a membrane electrode assembly (MEA; presented in Fig. 1) consisting of a porous anode, a cathode, and an electrolyte that can conduct protons. The working principle of PEMFCs is simple, i.e., air (oxygen) and fuel (hydrogen) are supplied at the cathode and anode sides, respectively. The H$_2$ molecules first flow from the anode to the gas diffusion layer and then reach the catalyst layer (CL). The CL is the site where hydrogen oxidation occurs to produce protons and electrons. The protons are carried by membrane electrolytes toward the porous cathode, whereas the electrons flow through the outer path and generate electricity. Oxygen undergoes reduction in the CL, resulting in the production of water as a by-product [5].

✉ Shakeel Ahmed
shakeel@haut.edu.cn

✉ Faizah Altaf
faizah.altaf@kfupm.edu.sa

[1] School of Material Science and Engineering, Henan International Joint Laboratory of Nano-Photoelectric Magnetic Materials, Henan University of Technology, Zhengzhou 450001, China

[2] Interdisciplinary Research Center for Hydrogen Technologies and Carbon Management, King Fahd University of Petroleum and Minerals, 31261 Dhahran, Saudi Arabia

[3] School of Materials Science and Engineering, Georgia Institute of Technology, Atlanta, GA 30332, USA

Fig. 1 Illustration of the major components of a proton exchange membrane fuel cell and its working principle
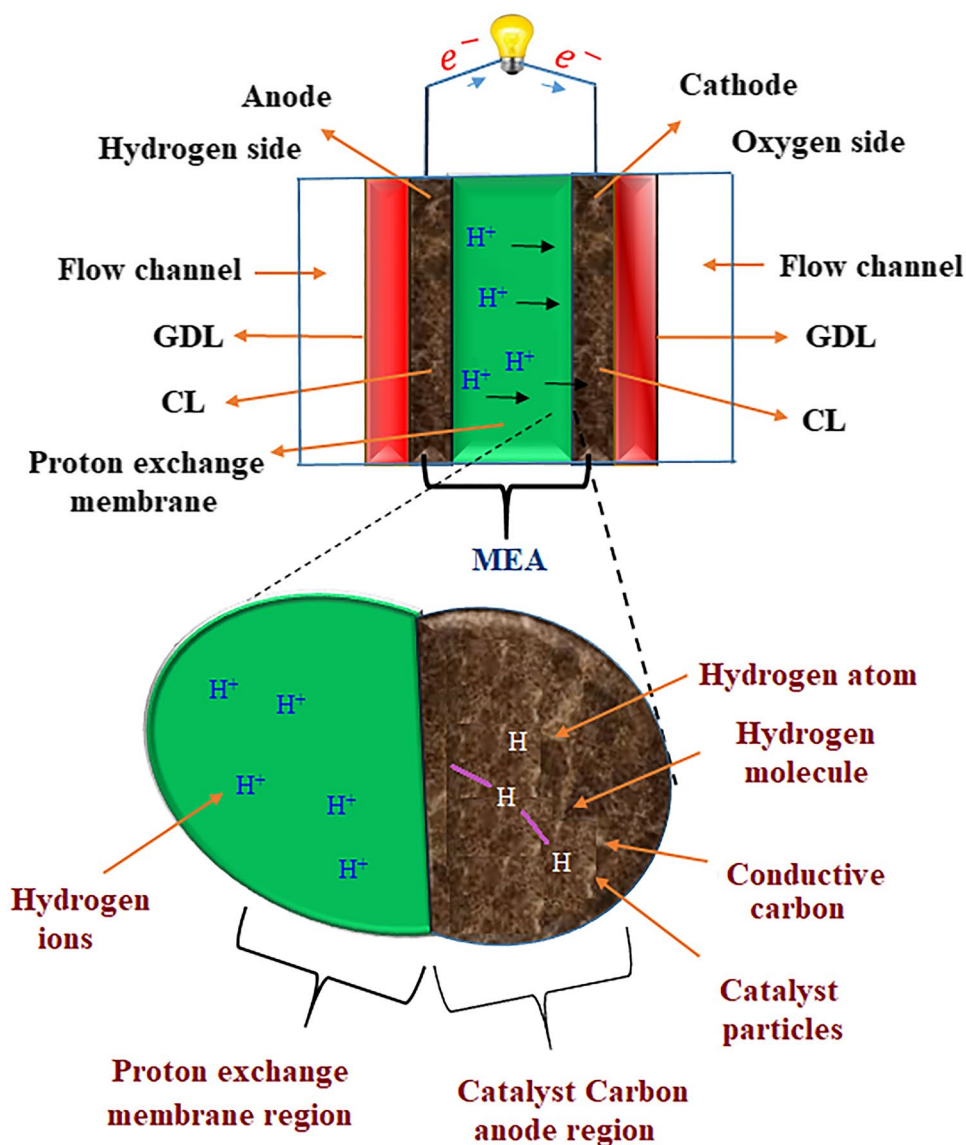
PEMFCs are widely regarded as one of the most promising power sources and offer several significant advantages [6, 7], such as compact design, high current prototype efficiency of up to 60%, fast start-up, excellent power densities (compared with batteries), long lifetime, eco-friendly exhaust, the capability to operate at low temperature, and the provision of the option for quick refueling [8]. These properties enable the commercialization of PEMFCs for transportation, as well as stationary and portable applications [9]. Despite these benefits, some noteworthy challenges are still present that hinder the commercialization of PEMFC technologies. The major challenges are high cost and reliability issues concerning the availability of suitable materials and components [10, 11].

Primary attention in proton exchange membrane (PEM) technologies has been focused on the modification and replacement of Nafion® membrane, mostly utilized for the development of PEM, also called polymer electrolyte membrane (the major component of PEMFCs) [12], because of some of its extraordinary characteristics, including chemical, mechanical, and electrochemical stabilities and high proton conductivity [13]. Indeed, Nafion® membranes are considered the standard PEMs, and the performance of all newly prepared composite membranes is compared with that of Nafion® membranes. However, some drawbacks of Nafion® membranes [14] (i.e., high fuel permeation, worsening of performance at high temperatures, high cost, and environmental incompatibility) motivate the discovery of alternate PEMs for PEMFCs [15]. Among them, organic–inorganic composite PEMs have attracted considerable attention. The functions of the inorganic component are to increase the mechanical, chemical, and thermal stabilities and membrane durability, enhance proton conduction, and reduce fuel permeabilities [16].

Polyvinyl alcohol (PVA) membranes have garnered considerable interest in applications of PEMFC because of their unique features and potential advantages, such as good chemical and thermal properties, high water absorption, flexibility, exceptional film formation, and cross-linking capacity. The hydroxyl (OH) group of PVA can be utilized for this purpose. These membranes can be easily synthesized and tailored to meet specific requirements, making them attractive for PEMFCs and direct methanol fuel cells [17, 18]. In PVA-based materials, the doped impurities perform the functions of the primary charge-transferring agent. Pristine PVA does not show high proton conductivity, and its maximum proton conductivity can reach 10^{-10} S/cm. Hence, to utilize PVA-based membranes in PEMFCs, proton conductivity must be induced through the incorporation of other materials and additional processing steps. Among them, sulfonation (using sulfonating agents), other material/morphological modifications (irradiation and chemical cross-linking, freezing, and heat treatment), or blending (with other conductive polymers) were proposed and used for this purpose [19, 20]. Another way to enhance the properties of PVA is the preparation of inorganic material-based PVA composite membranes, such as PVA/titania/PSSA [21], PVA/alumina [22, 23], PVA/silica [24], PVA/sulfanilic acid tethered poly(methyl vinyl ether-alt-maleic anhydride) [25], PVA/zirconium phosphate [26], PVA/MMT [27], and PVA/CNT [28] membranes.

Polyvinylpyrrolidone (PVP) is a widely used polymer in industrial applications because of its versatility and compatibility with N-heterocyclic compounds. In the realm of FC technology, PVP has been utilized in the synthesis of PEMs. However, pure PVP membranes tend to be brittle and hydrophilic, which can limit their effectiveness in practical applications. To address these limitations, PVP is blended with other polymers, which results in the formation of homogeneous composite electrolytes for PEMFCs with high mechanical strength and flexibility [29]. One notable example is the polyethersulfone (PES)–PVP composite membrane, where PVP is blended with PES. PES is an engineering thermoplastic with high mechanical properties and chemical inertness, making it an ideal material for enhancing the performance of PVP membranes [30]. Other blends include PVP with PVDF, which exhibited superb mechanical and thermal stabilities and the highest ionic conductivity of 0.093 S/cm [31]. PVP with PFSA is another blend that exhibited good proton conduction because of the acid–base interaction between the sulfonic acid (–SO$_3$H) and amino (–NH$_2$) groups of PFSA and PVP, respectively. Another system is the PVP–PVA composite with barium zirconate [32].

Carbon allotropes have been used in many electrochemical devices because of some specific features, such as their abundant supply, easy processability, good stability, and environmental versatility [29]. Graphene (G) is one of the most marvelous allotropes of carbon with sp^2 hybridization along with a two-dimensional (2D) monolayer lattice. G is composed of a thick sheet of single carbon atoms with a honeycomb arrangement. The excellent thermal, mechanical, and electrical characteristics of G make it useful in the field of materials science [33, 34].

Graphene oxide (GO) has been associated with notable improvements in the thermal, chemical, and mechanical properties of polymer matrix, even with low content. GO, a derivative of G, has the same carbon sheet but has additional functionalities, such as –COOH, −OH, C=O, and −O$^-$ anchored to its surface and edges [35]. These functionalities play a crucial role in promoting interfacial interactions between polymer matrix and filler, thereby enhancing the overall compatibility and performance of the composite material [36].

Moreover, GO serves as an effective inorganic filler in PEMFCs because of its distinctive properties [37]. With its substantial surface area and hydrophilic functional groups, GO promotes proton conduction through the hopping mechanism [38], which facilitates the movement of protons across the membrane and enhances the efficiency of the FC. Furthermore, the presence of GO in composite membranes enhances their water retention capabilities [39]. However, these properties of GO can be further improved by anchoring sulfonic acid groups (SO$_3$H) at its surface through sulfonation (acid functionalization). Free-standing GO has an ionic conductivity value of 0.04 S/cm at 303 K. However, by incorporating SGO within the polymer matrix, the ionic conductivity will further increase (because of the large number of SO$_3$H moieties). Higher water uptake and chemical and mechanical strengths of the resultant composite PEMs have also been observed [40]. GO can easily disperse in many polar and nonpolar solvents, such as water [41]. Heo and coworkers [42] have synthesized novel sulfonated graphene oxide (SGO)/sulfonated poly(ether ether ketone) (SPEEK) composite membranes by enhancing the interfacial interaction between SPEEK polymer and SGO filler by developing hydrogen bonds.

Hariprasad et al. [43] fabricated the SPVdF-HFP/SGO hybrid membrane and obtained better water uptake and proton conductivity than the pristine SPVdF-HFP membrane. In addition, the complex structure generated between SGO and membrane chains helps to lower the fuel crossover and swelling ratio of the hybrid membrane.

Beydaghi and colleagues [44] prepared composite membranes by incorporating aryl SGO into the PVA matrix and determined that the resultant composite electrolyte has enhanced proton conductivity and mechanical, chemical, and thermal stabilities. Chien and coworkers [45] claimed that GO/Nafion® nanocomposite membrane exhibited improved water content and increased proton conductivity (four times) compared with pristine Nafion®
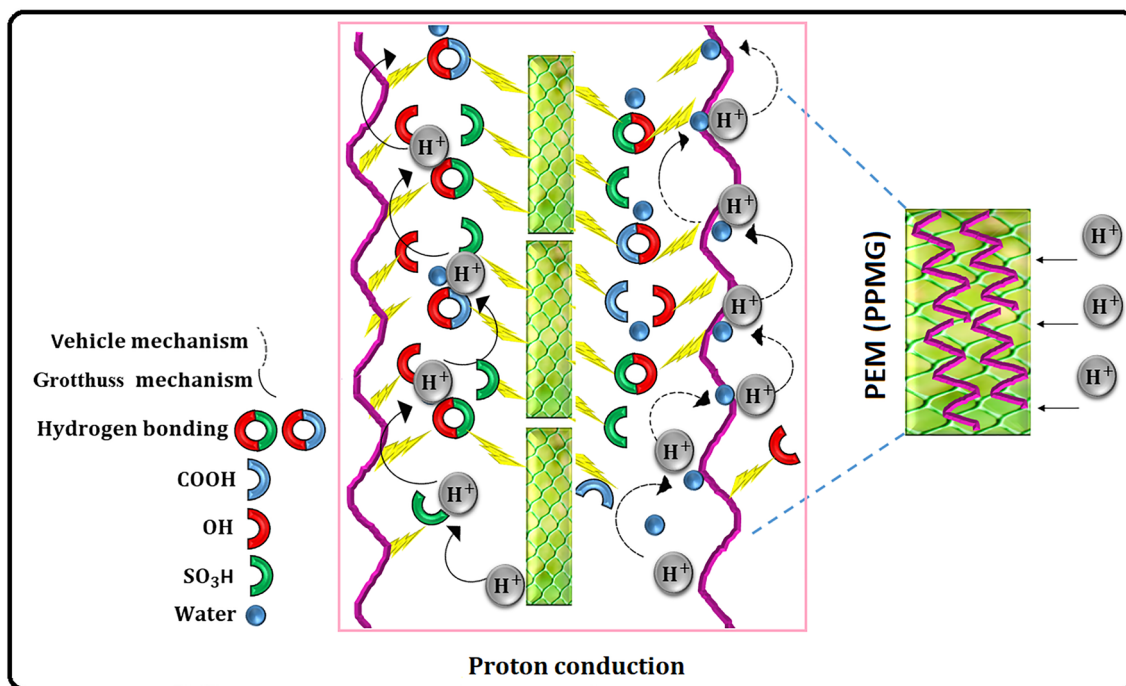
Scheme 1 Possible proton conduction mechanism for PPMG composite electrolytes

at 120 °C. Beydaghi and colleagues [44] also prepared nanohybrid PEMs composed of SPEEK/PVA/SGO/Fe_3O_4 that showed improved results in terms of 51.2 MPa tensile strength, 0.084 S/cm proton conductivity, and 122.7 mW/cm^2 power density. Zhang and coworkers [46] reported that SPEEK/DGO nanohybrid membrane exhibited increased ionic conductivity and single-cell performance results at higher temperatures compared with pristine SPEEK under anhydrous and hydrated environments. In their work, Pandey et al. [47] observed that nanohybrid membranes based on sulfonated imidized GO showed excellent stability and ionic conductivity.

Kumar et al. [48] prepared composite membranes by incorporating sulfonic acid-functionalized GO into SPEEK and obtained remarkable results in terms of proton conductivity (0.055 S/cm), cation exchange capacity (CEC; 2.3 meq/g), power density (378 mW/cm^2), and FC performance compared with that of pristine SPEEK membrane.

In the present work, a novel strategy for fabricating composite electrolytes for PEMFCs is reported, where we prepared PPMG-based electrolytes using a PVA–PVP blend and varying concentrations of sulfonated filler. The polymer blend was crosslinked using tetraethyl orthosilicate (TEOS). The structural and morphological characteristics of PEMs were characterized using Fourier transform infrared (FTIR) spectroscopy, X-ray diffraction (XRD), and scanning electron microscopy (SEM). The proton conductivities were measured using the independent method.
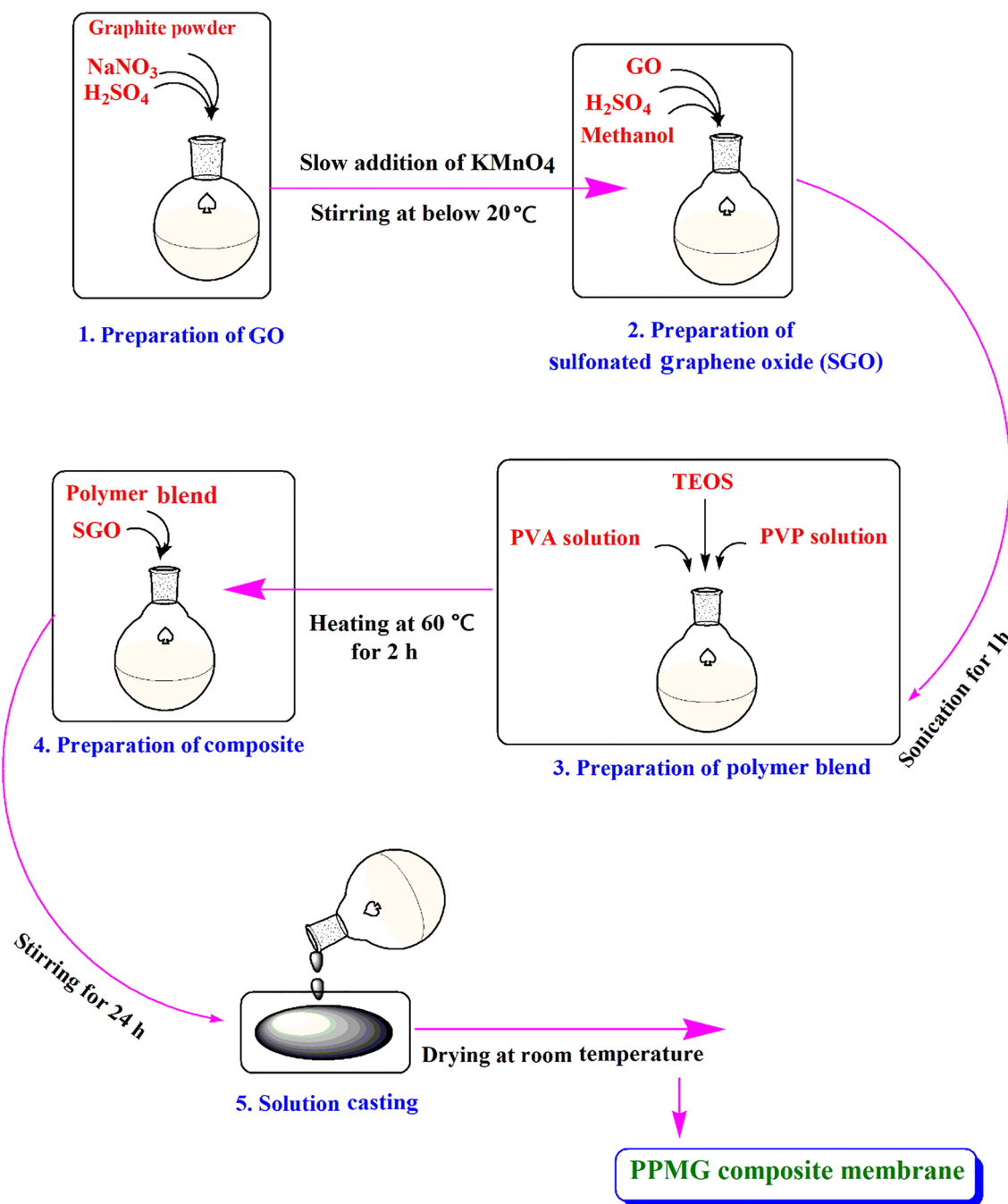
Experimental

Materials

PVA, graphite powder, hydrochloric acid (HCl), PVP, Nafion® (15%) solution, and isopropyl alcohol were obtained from Sigma-Aldrich and used as received without undergoing additional purification processes. Methanol (MeOH) and TEOS were purchased from Sigma-Aldrich and were of analytical grade. Potassium permanganate ($KMnO_4$), sulfuric acid (H_2SO_4), sodium nitrate ($NaNO_3$), sodium hydroxide (NaOH), and sodium chloride (NaCl) were of analytical reagent grade (Scheme 1).

Development of PPMG Composite Electrolytes

The depiction of the experimental setup for the preparation of PPMG composite electrolytes is given in Scheme 2 and involves the following steps:

Preparation of GO

The synthesis of graphite oxide from flake graphite powder via the modified Hummer's method [49] involves the oxidation of natural graphite using a mixture of strong acids and oxidizing agents, leading to the introduction of oxygen-containing functionalities to the G layers. Briefly, the process involved oxidizing graphite using $NaNO_3$ and H_2SO_4,

Scheme 2 Depiction of the experimental setup for preparation of PPMG composite electrolytes

specifically 200 mL of H_2SO_4 per 5 g of graphite served as the dispersion medium. To this graphite dispersion, 3 g of $NaNO_3$ was added, and the mixture was cooled to 0 °C using an ice-cold water bath. For 6 h, 25 g of $KMnO_4$ was gradually added. After completing the addition of $KMnO_4$, the resulting mixture was stirred at room temperature for an additional 6 h. The reaction was terminated by adding ice-cold water and 5% H_2O_2 to neutralize any remaining $KMnO_4$.

Then, the obtained graphite oxide was recovered and washed with deionized (DI) water and HCl(aq), followed by vacuum drying. Next, GO was produced by dispersing 5 g of graphite oxide in 50 mL of DI water and sonicated for several hours until the transparent solution was obtained. Subsequently, the GO solution was centrifuged at 4,000 r/min for 15 min to eliminate any unexfoliated GO particles. The resulting precipitates were washed with

water and HCl solution. Finally, the product was dried in a vacuum overnight for further use.

Synthesis of SGO

In this procedure, 30 mg of GO was introduced to a mixture of MeOH and 0.5 mol/L H_2SO_4 solution at 65 °C for 1.5 h. In the next step, 5 mL of 0.1 mol/L sodium nitrite solution was dropwise added, and the resulting mixture was maintained at 70 °C for a duration of 2 h to facilitate the reaction. Following the completion of the reaction, the mixture was washed, and the SGO nanoparticles were collected by centrifugation. Then, the collected particles were subjected to multiple washes with water until reaching a neutral pH [50].

Preparation of the Polymer Blend and Cross-Linking

To prepare the polymer blend, a predetermined concentration of PVP and PVA was carefully added to DI water. Then, the mixture was stirred thoroughly at the optimal temperature until a uniform blend was achieved, ensuring proper dispersion of the polymers within the solvent. Meanwhile, a separate solution of TEOS was meticulously prepared. Once the polymer blend reached the desired consistency, the TEOS solution was slowly introduced to the blend using a dropping funnel, enabling controlled incorporation of the silicate precursor. The composite mixture underwent thermal treatment, i.e., heated to 50 °C and maintained at this temperature for a duration of 4 h, enabling the initiation of chemical reactions between the polymer components and the silicate precursor, which promoted cross-linking and intermolecular bonding within the blend.

Following thermal treatment, the resulting mixture was filtered to remove any impurities or undissolved particles, ensuring the purity and homogeneity of the polymer blend. Subsequently, the filtrate was dried, yielding a solid product ready for further utilization in subsequent processing steps or applications.

Preparation of the Composite Electrolytes

The incorporation of SGO into the crosslinked PVA–PVP blend proceeded by adding SGO at five different weight percentages (i.e., 2 wt%, 4 wt%, 6 wt%, 8 wt%, and 10 wt%). Initially, GO was added to DI water and sonicated for 30 min. In the next step, a homogeneous GO solution was added to the PVA–PVP blend. The mixture was first stirred at 80 °C for 4–5 h and then sonicated for 30 min to ensure an even dispersion. After settling overnight to remove bubbles, the solutions were cast onto Petri dishes using a dissolution casting technique. Following evaporation at room temperature for 24 h, the membrane electrolyte was carefully extracted. The same process was repeated for all composite electrolyte PEMs. The resultant composite PEMs were labeled accordingly, i.e., 2PPMG, 4PPMG, 6PPMG, 8PPMG, and 10PPMG. The proposed reaction mechanism for PPMG composite electrolytes is presented in Scheme 3.

Membrane Characterizations

Fourier Transform Infrared Spectroscopy

The presence of functional moieties in pristine filler (GO), sulfonated filler (SGO), and PPMG samples was investigated using the FTIR spectrophotometer Nicolet 650 through the direct contact of the ATR tip with the samples. All spectra were recorded at 64 scans with spectral resolution in the range of 4000–400 cm^{-1}.

X-ray Diffraction

XRD was employed to examine the crystallographic structures of all synthesized samples. An X-ray powder diffractometer (D/Max-3A Rigaku) with Cu Kα radiation ($\lambda = 1.5418$ Å), 35 kV voltage, and 30 mA current was used to record the XRD patterns at ambient temperature.

Scanning Electron Microscopy

The scanning electron micrographs were taken using the LEO 1530 scanning electron microscope. The prepared samples were sputtered with gold for approximately 120 s before SEM analysis to ensure that the sample surface did not have a charge.

Atomic Force Microscopy

Atomic force microscopy (AFM; Bruker MM8, USA) was employed to examine the surface morphology of the coatings and evaluate their surface roughness. Imaging was conducted in tapping mode, covering areas of 1×1 μm. The images were initially fitted to the first-order x–y plane and subsequently flattened using the Nanoscope software (v1.30). Surface roughness measurements were conducted based on the root-mean-square (RMS) roughness values at various locations on each sample. For each coating, 10 scans of different areas were analyzed to quantify surface roughness.

Water Uptake

To determine their water uptake capacities, all composite electrolyte samples were vacuum-dried at 50 °C for 5 h. The weight of the fully dried samples was measured and recorded. Subsequently, the dried samples were soaked in
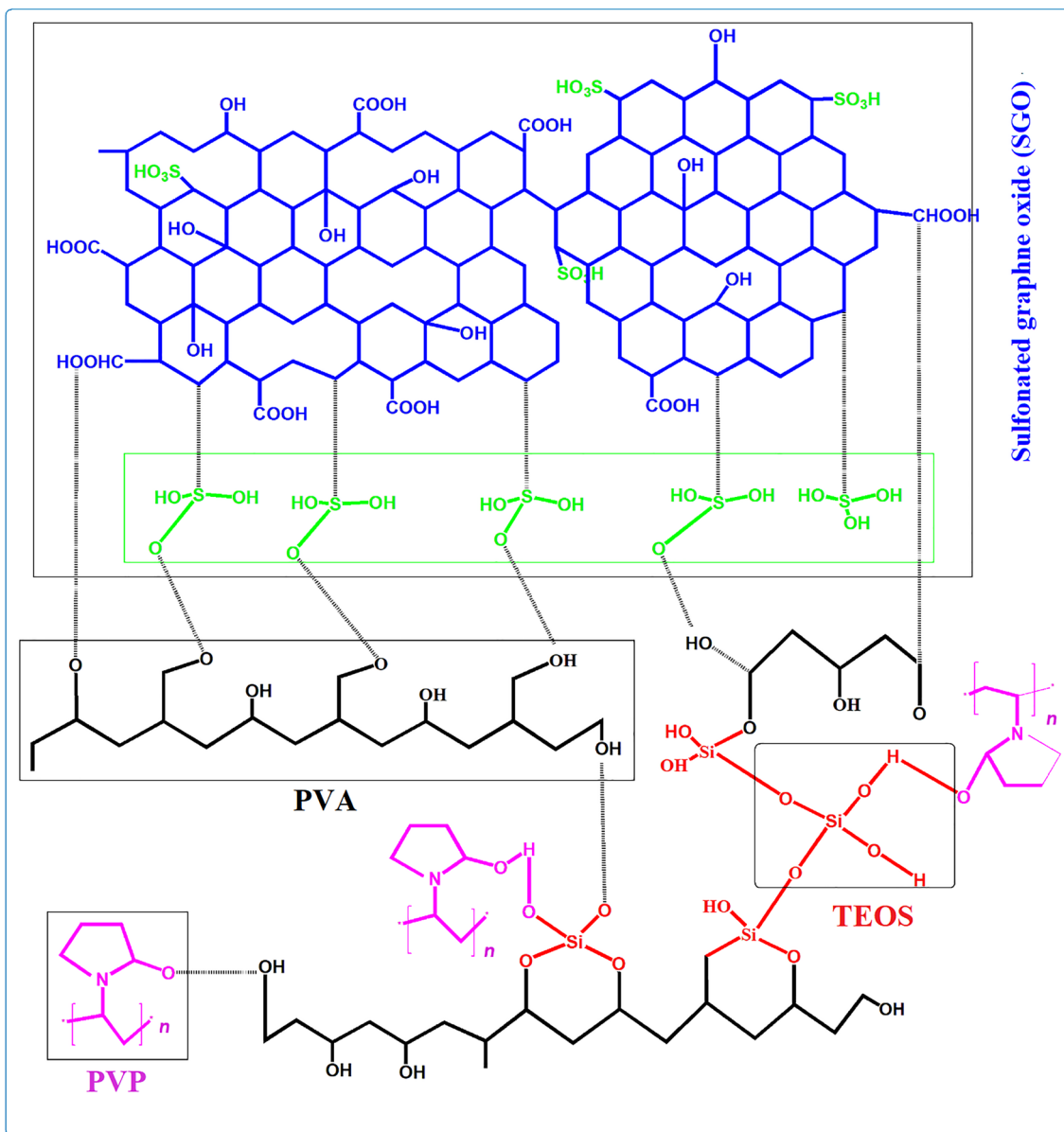
Scheme 3 Proposed reaction mechanism for PPMG composite electrolytes

DI water at ambient temperature for 24 h. After soaking, any water content on their surface was carefully eliminated using tissue paper before weighing again.

The water uptake capacity was calculated using Eq. (1):

$$\text{Uptake} = \left[\frac{W_w - W_d}{W_d}\right] \times 100\% \qquad (1)$$

where W_w and W_d were the masses of the dried and wet samples, respectively.

Swelling Percentage

The swelling behavior of composite electrolytes in the presence of water was evaluated by comparing their lengths in the wet and dry states. Initially, the electrolyte samples were dried at 50 °C overnight before their lengths were measured. In the next step, the dried samples were submerged in DI water for 10 h at room temperature. Following this, the wet samples were dried carefully with

the help of tissue paper, and their lengths were evaluated once more.

The swelling ratio (SW) for each PEM was subsequently calculated using Eq. (2):

$$SW = \left[\frac{(L_w - L_d)}{L_d} \right] \times 100\% \tag{2}$$

where L_w is the wet membrane length, and L_d is the dry membrane length.

Cation Exchange Capacity

The CEC values of all electrolyte samples were assessed by the traditional acid–base titration method. Initially, a piece of the sample was added to a 50 mL solution of 1 mol/L NaCl for 1 day. This step aimed to prompt an ion exchange reaction, wherein H^+ ions from the membrane electrolyte would replace Na^+ ions in the solution. Following this, the solution containing the liberated H^+ ions was subjected to titration employing a 0.01 mol/L NaOH solution. Throughout the titration process, phenolphthalein functioned as the indicator to detect the titration endpoint. To ensure the reliability of the results, each measurement was repeated at least three times until a consistent titration endpoint was achieved.

The CEC was calculated using Eq. (3):

$$CEC = \frac{(V_{NaOH} \times C_{NaOH})}{W_d} \tag{3}$$

where CEC is the cation exchange capacity (meq/g); V_{NaOH} is the volume of added titrant (mL), C_{NaOH} is the molar concentration of the titrant; and W_d is the mass of the dried sample (g).

Proton Conductivity Analysis

The proton conductivities of all prepared composite electrolytes were determined by employing the alternating current (AC) impedance method. Each membrane sample was first activated by immersing in a 2 mol/L H_2SO_4 solution at ambient temperature and then rinsed with DI water. Each activated electrolyte was placed between two platinum electrodes. Subsequently, resistance measurements were performed across frequencies spanning from 100 kHz to 10 Hz, employing an AC amplitude of 5 mV. The measurements were conducted at temperatures ranging from 25 °C to 80 °C within dry O_2 and H_2 atmospheres. Each prepared electrolyte underwent testing five times to ensure reliability. The reported conductivity values represent the average of measurements taken from four different samples.

The ionic conductivity values were calculated using Eq. (4):

$$\sigma = \frac{L}{RA} \tag{4}$$

where σ is the proton conductivity (S/cm), L is the thickness (cm) of the membrane, R is the resistance derived from impedance data, and A is the cross-sectional area (cm^2) of the membranes.

Cell Design for FC Performance

The single-cell performance test was conducted by developing MEA using the catalyst-coated electrode method, and results were obtained by analyzing the polarization curves. A design featuring interdigitated flow fields was employed in this study. In this design, the flow channels are terminated, enabling the reactant to flow through the porous reactant layer under pressure. This setup effectively removes water from the electrode structure, preventing flooding and boosting the overall performance of the cell. In addition, the flow field design induces forced convection, addressing concerns related to flooding and gas diffusion limitations and ultimately enhancing the efficiency of the FC [51]. The catalyst ink was synthesized by mixing Pt/Ru/C catalyst (60% Pt/Ru and 40% C) for the anode and Pt/C catalyst (60% Pt and 40% C) for the cathode, along with a 15% solution of Nafion® binder and DI water. Following this, the ink was applied to a carbon cloth and then dried and baked at 100 °C for a duration of 15 h.

The prepared composite electrolytes were sandwiched between two electrodes. The anode consisted of 0.2 mg/cm^2 of Pt/Ru/C, while the cathode consisted of 0.2 mg/cm^2 of Pt/C. Following this, the assembly underwent hot pressing at 60 °C under 100 kg/cm^2 pressure for 10 min to form MEA. The electrochemical performance of PEMFCs was evaluated under ambient pressure conditions, with H_2 gas supplied at a rate of 100 mL/min and O_2 gas supplied at a rate of 80 mL/min. These assessments were conducted at temperatures of 25 °C and 70 °C.

Results and Discussion

Fourier Transform Infrared Spectroscopy

Figure 2 presents the FTIR results of pristine GO, SGO, and PPMG membranes. Pristine graphite shows weak infrared peaks at 1573 cm^{-1} corresponding to the C=C bond because of high symmetry. However, this peak in GO appeared at 1570 cm^{-1} and became sharper because of the asymmetry of GO (Fig. 2a Plot i), as the sonication and use of Hummer's method disrupt the symmetry of graphite [52]. The band at 1399 cm^{-1} corresponds to the skeletal vibrations of C–O–C and C–OH in the oxidized graphitic
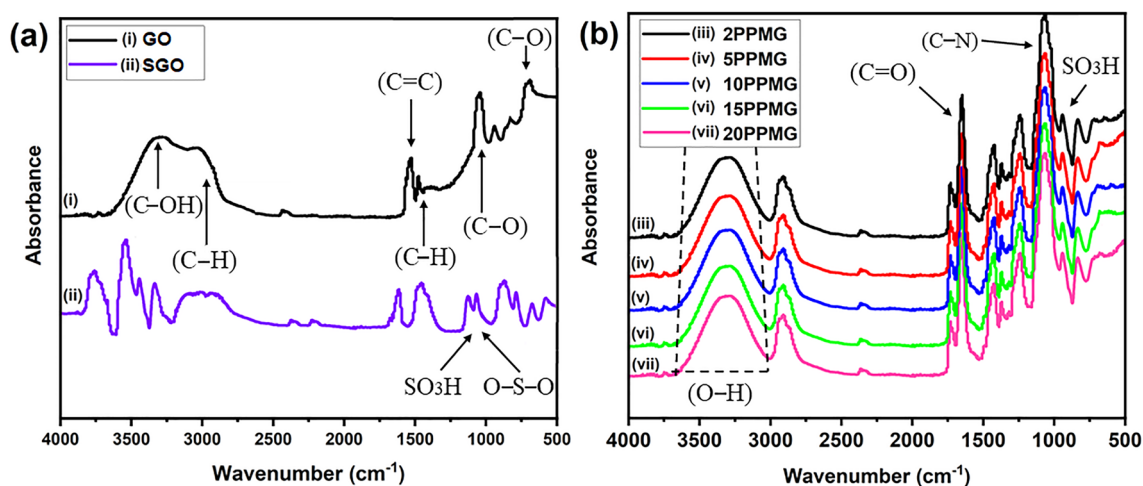
Fig. 2 FTIR spectra of **a** graphene oxide (GO), sulfonated graphene oxide (SGO), and **b** PPMG electrolytes

phase [53]. Figure 2a (Plot ii) shows the FTIR spectrum of SGO. The process of sulfonation generates a functional group at the surface of GO, which is shown by the appearance of new bands at 1292 and 1172 cm^{-1} attributed to the sulfonic acid (SO$_3$H) group of SGO [42]. The band that appeared at 3833 cm^{-1} relates to –OH groups of PEMs. The broad bands that appeared at 3401 and 3418 cm^{-1} in both spectra are attributed to the stretching vibration of OH moieties [54]. The band observed at 2955 cm^{-1} becomes broad because of the O–H stretch (acidic group) in sulfonated filler [55].

Pure PVA shows a characteristic peak at 3254 cm^{-1}. In the case of composite electrolytes, the broad band observed at 3002–3510 cm^{-1} is attributed to the stretching vibration of PVA hydroxyl groups (OH) (Fig. 2b Plot iii). The high-intensity –OH band detected in all prepared electrolytes is attributed to the occurrence of hydrogen bonding among C=O (PVP), OH (PVA), and SGO. The –OH stretching band is highly dependent on hydrogen bonding [56], shifts to a lower wavenumber, and broadens when the SGO content is increased (Fig. 2b Plot iv). As the filler content was further increased, the O–H bond changed into S–O–H, causing the band to constantly broaden (Fig. 2b, Plot v) with the increase in SGO content (Fig. 2b Plots vi and vii).

The band that appeared at 2910 cm^{-1} is associated with the C–H stretching vibration of PVA. The distinguishing vibration bands that appeared at 1650 and 1245 cm^{-1} are attributed to the C=O and C–N stretching vibrations of the PVP polymer [57, 58]. The band at 1733 cm^{-1} confirmed the presence of such free C=O moieties but appeared to be hidden by the vicinity bands [59, 60]. The sharp band observed at 1062 cm^{-1} is attributed to sulfonic acid (SO$_3$H) stretching [61]. This band becomes broader and thicker with the increase in filler content (2–10 wt%). The Si–O–Si band at 1062 cm^{-1} is attributed to the formation of a fresh covalent

bond by the condensation reaction that occurred between C–OH (PVA) and Si–OH (hydrolyzed TEOS) [62].

X-ray Diffraction

The XRD pattern of graphite typically shows a sharp and intense peak at approximately $2\theta = 26°$, corresponding to the (002) plane of graphite, which represents the interlayer spacing between G layers. Natural graphite shows a highly ordered crystal framework having a 0.34 nm layer-to-layer gap. However, after employing Hummer's method, the peak that appeared at $2\theta = 26°$ expanded, and an additional peak detected at $2\theta = 11.10$ (001) was attributed to GO, as shown in Fig. 3a Plot i.

The d-spacing (interlayer spacing) was determined using Bragg's law ($\lambda = 2d\sin\theta$) and was 0.80 nm, confirming the presence of oxygen in the network of G sheets [63]. This increase in the value of d-spacing is attributed to the addition of oxygen-containing functionalities between layers. Figure 3a Plot ii showed that sulfonation of GO results in a peak shift from $2\theta = 11.10°$ to $2\theta = 26.9°$ (002) having $d = 0.52$ nm. The reduction of d-spacing values after sulfonation is related to the fact that sulfonation removes oxygen functional moieties and causes restacking of exfoliated GO sheets because of the π–π interaction. The peak shifting toward the higher 2θ value is attributed to the presence of the SO$_3$H group of sulfonated filler [64].

The XRD spectrum of pure PVA exhibits two peaks, i.e., a small peak at $2\theta = 36°$ indicating the presence of a crystalline phase with a certain arrangement of polymer chains and a broad peak at $2\theta = 21°$, indicating the existence of an amorphous phase [65]. The blending of PVA with PVP leads to a decrease in the intensity of the PVA peak and an increase in the amorphous nature of the resultant composite membrane [66].
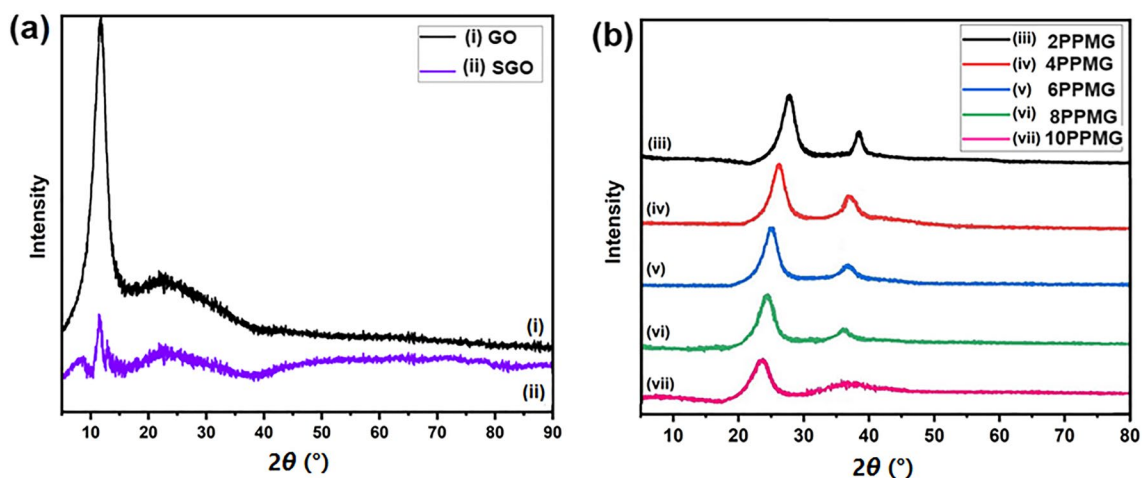
Fig. 3 XRD patterns of **a** GO, SGO, and **b** PPMG composite electrolyte/membranes

Upon the addition of 2 wt% filler to polymeric blends, the peak intensity decreases, and the peak broadens (Fig. 3b Plot iii). A further decrease in the peak intensity occurred with the increase in SGO content from 4 wt% to 10 wt% (Fig. 3b Plots iv, v, vi, and vii). This phenomenon can be attributed to the establishment of hydrogen bonds between the –SO$_3$H groups of the nanofiller and the –OH groups of the polymer matrix [67]. The occurrence of such interactions enhances the intermolecular bonding within the system, resulting in a decrease in the crystalline phase and an expansion of amorphous regions [68]. These amorphous regions lower the energy barrier and enhance the segmental motion of

the polymer chain, consequently leading to increased ionic conductivity. Interestingly, the XRD spectra do not exhibit peaks associated with SGO because of its inherently amorphous nature.

Scanning Electron Microscopy

The SEM micrographs of GO, SGO, and the prepared composite PEMs are shown in Fig. 4. Both GO and SGO have different morphologies. Figure 4a shows that GO has a thin, transparent nanosheet 2D structure with a wrinkled or crumpled morphology [69]. These sheets vary in size and shape,
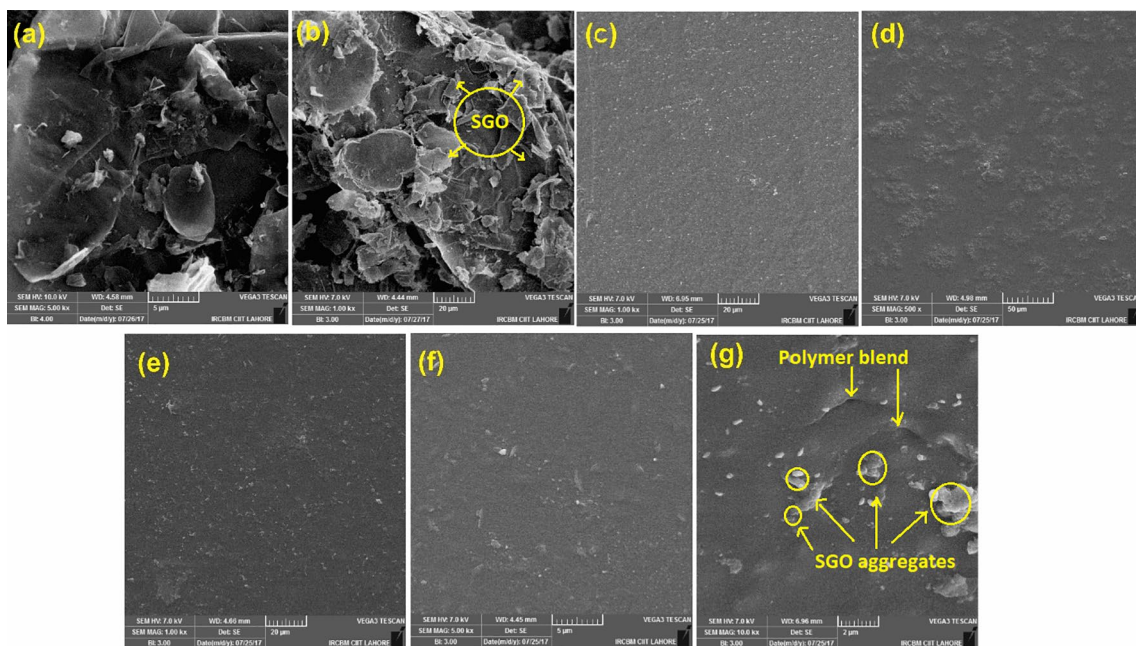
Fig. 4 SEM images of **a** GO, **b** SGO, **c** 2PPMG, **d** 4PPMG, **e** 6PPMG, **f** 8PPMG, and **g** 10PPMG composite electrolyte/membranes

and the edges of the GO sheets often appear irregular or jagged because of the oxidation process. In addition, the SEM images revealed some degree of aggregation or face-to-face stacking of the sheets, resulting in overlapping layers. GO was functionalized using H_2SO_4 as the sulfonating agent. Figure 4b shows that SGO also has a 2D structure even after functionalization but has foreign matter covering its surface [70]. A comparison between GO and SGO indicated that the surface of SGO appeared rougher than that of GO, likely because of the functionalization process.

PVA is known for its highly hydrophilic nature, and the SEM images show a smooth and uniform surface with no distinct features or irregularities. The surface morphology may appear homogeneous, with a lack of visible pores or voids [71]. The incorporation of SGO into the PVA–PVP blend leads to the emergence of whitish nano-moieties at the surface of the resultant composite PEMs, thereby confirming the successful integration of sulfonated filler into the polymer matrix. Here, we used different weight percentages of SGO nanoparticles (2–10 wt%) to incorporate into the prepared polymer blend. The SEM results revealed the uniform dispersion of nanofillers within the blend membrane, which can be attributed to the formation of hydrogen bonding between filler and polymer matrix [72, 73]. The existence of SO_3H groups might accelerate the nanofiller dispersion within the polymer matrix and provide more proton pathways [74]. However, by increasing the amount of SGO, agglomeration of fillers occurred at the surface of the membrane, similar to other inorganic fillers [75].

Figure 4c, d illustrates that, at lower filler content, the PPMG composite membranes are homogeneous. By contrast, the PPMG composite membranes are no longer homogeneous in Fig. 4e. Noteworthy agglomerations of SGO nanoparticles were observable (Fig. 4f). The higher amount of SGO fillers results in the formation of agglomerates at the surface of nanocomposite PEMs, thus leading to poor dispersion of SGO in the PVA–PVP blend, mainly when the filler content is over 6 wt% (Fig. 4g). The poor dispersion of SGO is clear from the presence of several large uneven SGO agglomerates that are randomly scattered on the top surface, indicating that the SGO nanofillers were thoroughly dispersed throughout the polymer matrix. The agglomeration of nanofiller leads to a reduction in the active surface area, resulting in decreased membrane water content and, consequently, lower proton conduction. To prepare a homogeneous and fully dispersed composite polymer membrane, controlling the contents of the polymer and inorganic filler is necessary [76, 77].

Atomic Force Microscopy Analysis

The surfaces surface roughness of PPMG composite PEMs was compared by analyzing the roughness parameters,

Table 1 Surface roughness parameters of the prepared PPMG composite PEMs obtained from the AFM images

Sr. No.	Membrane type	Surface roughness (S_a (nm))	Root-mean-square roughness (S_q)
1	PVA	7.51	10.10
2	PVA–PVP	31.20	41.20
3	2PPMG	58.60	65.12
4	4PPMG	68.45	79.43
5	6PPMG	76.31	83.56
6	8PPMG	81.43	89.00
8	10PPMG	88.23	93.05

including average roughness (S_a) and RMS roughness (S_q) (Table 1). The AFM images were obtained in tapping mode, and the samples were affixed to glass slides using adhesive tape. The AFM images and line mapping of the PVA–PVP blend and composite PEMs are presented in Fig. 5.

The pristine PVA polymeric PEM exhibits a relatively smooth surface topography with low average roughness (S_a) and RMS roughness (S_q) values [78], as shown in the AFM images. However, when PVA is blended with PVP and crosslinked with TEOS, the surface roughness parameters increase significantly. Furthermore, in the case of composite PEMs, where different weight percentages of SGO were incorporated into the polymer blend, an increase in surface roughness is observed. Specifically, the S_a value of the composite PEM membranes is higher than that of the pristine PVA membrane. The surface roughness associated with the composite PEM is an order of magnitude higher than that of the pristine PVA membrane. The increased surface roughness of the composite membranes is attributed to the incorporation of the SGO component, which introduces nanoscale convolutions and topographical features to the membrane surface.

For the pristine PVA membrane, the values of S_a and S_q are low, while for PPMG composite PEMs, the values of S_a and S_q are high, which confirmed that the introduction of nanofiller (SGO) to the PVA–PVP blend caused surface roughness to increase significantly. PVA exhibits narrow hydrophilic channels, yielding a smooth surface with low roughness. Conversely, the inclusion of SGO nanoparticles that effectively occupy these channels in the polymeric matrix leads to increased roughness. The connection between hydrophilic and hydrophobic domains establishes clear ionic pathways for proton or water transport within the hybrid membrane. Consequently, PPMG composite membranes improve water sorption by generating hydrophilic nanodomains, which serve as fresh active sites for water retention, thereby aiding proton transport across different humidity levels. However, at higher loading, SGO
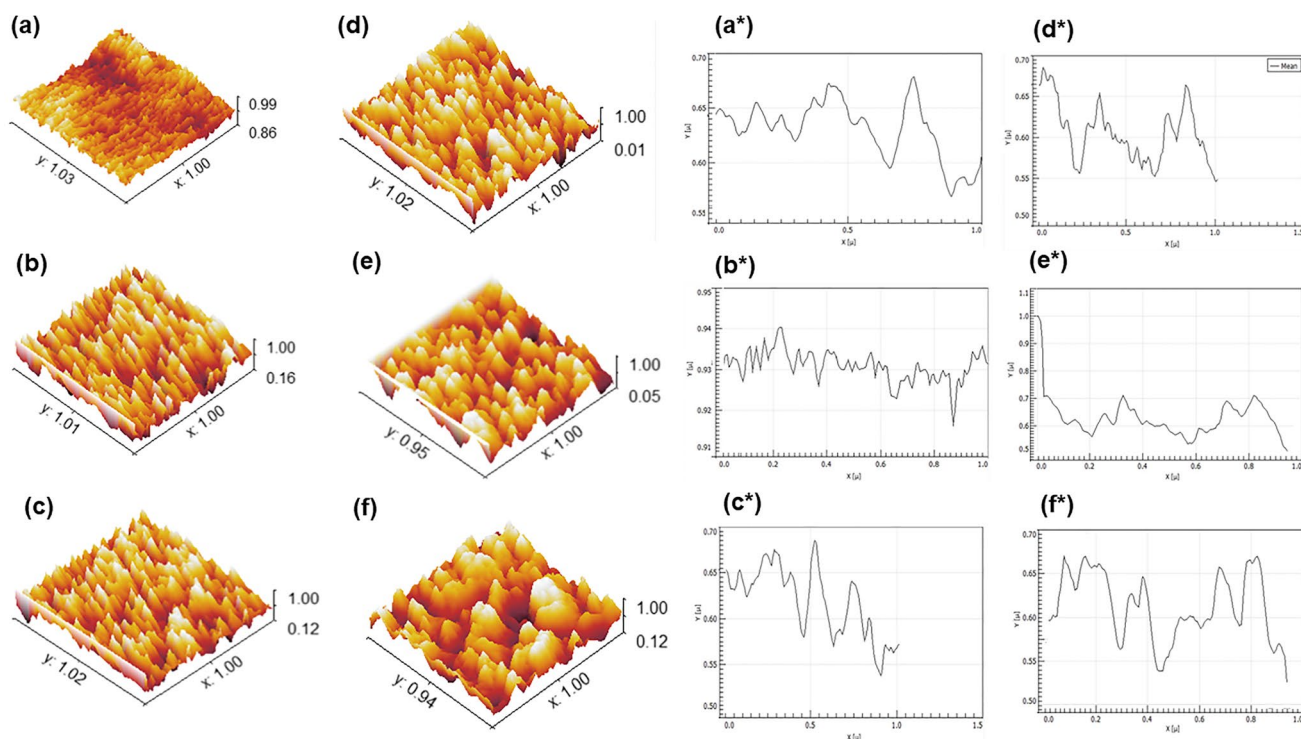
Fig. 5 AFM images of **a** PVA–PVP blend, **b** 2PPMG, **c** 4PPMG, **d** 6PPMG, **e** 8PPMG, and **f** 10PPMG. Line mapping of **a*** PVA–PVP blend, **b*** 2PPMG, **c*** 4PPMG, **d*** 6PPMG, **e*** 8PPMG, and **f*** 10PPMG composite PEMs

nanoparticles tend to aggregate with each other and result in lower water uptake and ionic conductivity.

The AFM results showed that the surface of the composite was rough ($S_a = 88.23$ nm for 10 wt% GO), while the surface of the PVA–PVP blend membrane was relatively smooth ($S_a = 31.2$ nm). In addition, the S_q also increased from 10.10 nm for the PVA membrane to 93.05 nm for the PMMG composite with an SGO content of 10 wt%.

The increase in the S_q stems from the strong compatibility between PVA, PVP, and SGO alongside the uniform dispersion of SGO within the blend matrix. This compatibility is attributed to the abundance of oxygen-containing functional groups on the surface of GO, fostering strong hydrogen bonding with polymer chains.

Water Uptake Determination

Water uptake refers to the absorption or uptake of water molecules by a material. In the context of FCs, water uptake typically refers to the process by which a membrane absorbs water molecules [79]. In PEMFCs, water plays a vital role in the proton transfer mechanism because water molecules within the FC environment contain protons in the form of hydronium ions (H_3O^+) and H_5O_2, which are critical for the proton transport process. These protons are transferred through the membrane electrolyte via ionic channels, which are typically hydrogen-bonded, and through a cationic mixture. Indeed, the presence of a sufficient hydration level in membrane electrolytes is crucial for achieving high proton conduction. Proper hydration guarantees a sufficient supply of water molecules, which is essential for facilitating the movement of protons through the membrane, thereby enhancing the overall performance of the FC.

However, excessive water uptake by the polymeric membrane can lead to detrimental effects, such as extreme swelling. When the membrane absorbs an excessive amount of water, it can swell beyond its designed dimensions. This swelling not only compromises the mechanical properties of the membrane but also negatively impacts its dimensional stability. Decreases in mechanical properties, such as tensile strength and elasticity, can result in membrane deformation or even rupture under operational conditions.

Furthermore, changes in dimensional stability can lead to issues, such as membrane delamination or distortion, which can impair the overall functionality and longevity of the FC. Therefore, adequate hydration is essential for optimal proton conductivity, and water uptake needs to be controlled within the membrane to prevent excessive swelling and maintain mechanical integrity and dimensional stability, which can be accomplished through the careful design of the membrane material and structure, as well as the implementation of effective water management strategies in FC systems [80].

Water uptake affects some of the properties of the membrane, such as dimensional stability and cation selectivity. Several parameters that can influence water uptake include the degree of sulfonation, membrane pretreatment, hydration and humidity level, and water temperature [81, 82]. Pure PVA shows high water uptake because of its hydrophilicity; however, its water uptake is affected by the addition of cross-linkers, induction of inorganic fillers, and creation of blends with other polymers to make PVA thermally and mechanically stable and induce proton conductivity [82].

The prepared PPMG composite electrolytes exhibit less water uptake compared with pure PVA membranes. Figure 6a shows that, among all samples, pure PVA membrane has the highest value of water uptake, i.e., 64%. The water uptake tended to decrease after the introduction of filler content and will continuously decrease with the increase in filler content. 2PPMG (2 wt% filler content) had the highest water uptake value of 51.6%, while 10PPMG (10 wt% filler content) had the lowest water uptake value of 44.8% because the $-SO_3H$ moieties of the nanofiller interact with

the $-OH$ groups of the polymer and develop hydrogen bonds, hence enhancing the interfacial strength and compactness of the membrane structure [83, 84], which, in turn, causes the constriction of water-transferring channels and decreases the water uptake.

In addition, when TEOS is used for cross-linking of the polymer matrix it also decreases the water uptake values by increasing the mechanical stability of the resultant PEMs [85]. The inclusion of PVP has been observed to have a limiting effect on the mobility of free polymer chains within the membrane structure. This phenomenon contributes to a reduction in water uptake by the membrane.

Swelling Percentage Measurement

The swelling of a polymer membrane refers to its capability to absorb and retain solvent molecules, typically water, which increases its volume. This phenomenon occurs because of the interaction between the polymer chains and
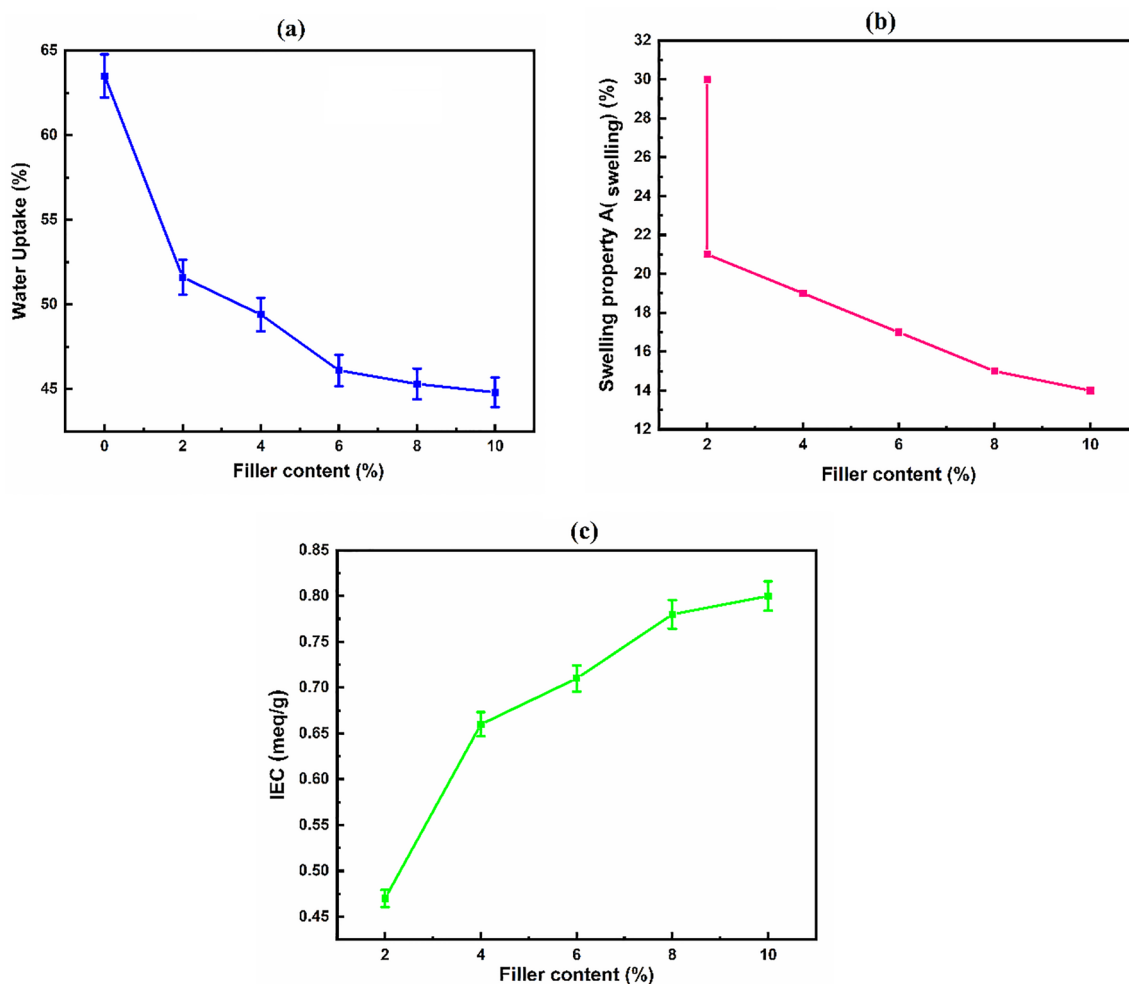
Fig. 6 **a** Water uptake percentage, **b** swelling percentage, and **c** ion exchange capacity of samples vs. filler weight percentage

the solvent molecules, which causes the polymer chains to expand and separate from one another.

Swelling can have both negative and positive impacts on the performance of the polymer membrane. On the one hand, swelling can enhance the transport properties of membranes, such as ionic conductivity, by increasing the availability of pathways for the diffusion of solutes, which is particularly important in applications such as FCs, where effective ion transport is key for device performance. On the other hand, excessive swelling can lead to negative consequences. For instance, excessive swelling can cause mechanical instability and dimensional changes in the membrane, leading to deformation or even rupture, which can compromise the integrity and functionality of the membrane, impacting its long-term durability and reliability. Therefore, controlling the swelling behavior of polymer membranes is important for optimizing their performance in various applications and can be achieved through the careful selection of polymer materials and adjustment of the membrane composition and structure to achieve the desired balance between swelling and mechanical properties. In addition, the implementation of appropriate water management strategies can help mitigate the effects of excessive swelling in applications where water uptake is a concern.

The swelling behavior of polymers in water is indeed influenced by their water uptake capacities, which, in turn, are determined by their inherent hydrophilic or hydrophobic nature. Hydrophilic polymers have a strong affinity for water molecules because of the presence of polar or ionic functional groups in their chemical structure. When placed in an aqueous environment, these polymers readily absorb water, leading to swelling. The water molecules interact with the polar groups in the polymer chains through hydrogen bonding, causing the polymer chains to separate and the overall volume of the polymer to increase.

By contrast, hydrophobic polymers repel water molecules and exhibit limited water uptake. These polymers have nonpolar chemical structures that are incompatible with water. As a result, these polymers tend to swell to a lesser extent or may not swell at all in water.

Figure 6b shows that pure PVA membrane has the highest swelling percentage of 30% because of its hydrophilic nature. However, when PVA is blended with PVP and reinforced with sulfonated inorganic filler (SGO), the swelling percentage gradually decreases from 21 to 14% with the increase in the amount of nanofiller (i.e., 2 wt% to 10 wt%) because of the formation of hydrogen bonds between –SO$_3$H and OH groups of the fillers and matrix, which leads to the formation of composite membrane with good dimensional stability [83].

The degree of swelling exhibited by a polymer in water is directly proportional to its water uptake capacity, which is determined by several factors, such as the density and distribution of hydrophilic or hydrophobic groups within the polymer structure. By controlling these factors, the swelling behavior of polymers can be tailored for specific applications, such as drug delivery systems, biomaterials, and membranes for separation processes [86].

Cation Exchange Capacity

CEC indicates the presence of exchangeable ions in the membrane. CEC is a secondary and reliable means of proton conductivity and provides information about the number of ionizable hydrophilic groups, typically sulfonic acid groups (–SO$_3$H), present in the membrane matrix. These ionizable groups are responsible for facilitating proton conduction in PEMs by providing sites for proton transport.

The CEC of a PEM is typically expressed in units of milliequivalents per gram and indicates the density of ionizable groups within the membrane matrix. A higher CEC value indicates a higher concentration of ionizable groups and, consequently, a greater potential for proton conduction. Therefore, materials with high ion exchange capacity (IEC) values have a greater potential for proton uptake and, consequently, exhibit enhanced proton conductivity, which is vital for achieving efficient proton transport within PEMFCs, ultimately leading to improved FC performance. Thus, selecting membrane materials with high IEC values is crucial for optimizing the proton conductivity and overall efficiency of PEMFCs [87, 88].

A previous study [89] reported that the CEC value of GO-based composite membranes increases with the increase in GO content but is lower than that of SGO-based (SGO-functionalized) membranes because of the absence of SO$_3$H groups. The presence of SGO in the polymer matrix improves hydrophilicity and increases sulfonating sites, hence increasing the membrane proton carrier capacity [53, 90].

Figure 6c shows that the CEC values of composite PEMs increased uniformly and continuously with the increase in SGO content from 2 wt% to 10 wt%. The maximum CEC value of 0.8 meq/g was obtained with 10PPMG. This phenomenon is attributed to the high filler content, which leads to an increase in the number of SO$_3$H groups, hence the high CEC value. This increasing CEC trend initially coincides with the increase in proton conductivity observed with the inclusion of SGO. This correlation indicates the contribution of SGO to proton conduction by augmenting sulfonic acid groups, which are pivotal as proton donors and carriers within the membrane.

Notably, sulfonated membranes boast exceptional water retention, which is crucial for efficient proton transport mechanisms, such as the Grotthuss mechanism and vehicular transport. Sulfonated PEMs retain more water, which serves as a medium for proton transfer. As a result,

sulfonated membranes have a high capacity for exchanging ions. In addition, this capacity increases as the SGO content increases. Thus, more functional groups are available for exchange because of the higher density of ionic sites distributed inside the polymer chains. However, after the addition of 6 wt% filler, the conductivity of the membranes decreased because filler agglomerates have a lower charge density than the matrix, which prevents cations from easily passing through the membrane [67, 91].

Higher SGO levels cause the SGO nanoparticles to clump together rather than dissolve into the polymer blend, which increases the barrier to proton transport and prevents proton conduction. An increase in SGO concentration causes the free volume that can be associated with water molecules to diminish, which is followed by a reduction in the size of the interconnected proton channels. Water has an impact on proton conductivity. Moreover, aggregated SGO nanoparticles hinder the passage of ions and reduce the movement of polymer chains. Notably, the addition of the SO_3H groups to these PEMs increases the CEC value but does not directly increase the proton conductivity.

The obtained water uptake, CEC, and swelling percentage values of the prepared PPMG composite membranes are compared with those of the composite membranes reported in Table 2.

Conductivity Measurements

Figure 7a depicts the proton conduction behavior of all synthesized PPMG composite electrolytes across a temperature

Table 2 Comparison of the water uptake, ion exchange capacity (IEC), and swelling percentage values of various composite membranes

| Membranes	IEC	Water uptake	Swelling (%)	References
2PPPMG	0.47	51.6	21	Present work
4PPPMG	0.66	49.4	19	Present work
6PPPMG	0.71	46.1	17	Present work
8PPPMG	0.78	45.3	15	Present work
10PPPMG	0.80	48.8	14	Present work
Nafion 212	0.89	46.3	–	[92]
Nafion 112	0.90	19.3	–	[92]
Crosslinked	0.612	–	–	[92]
Nafion/PVA	26.4 ± 0.1	0.47 ± 0.1	0.0	[92]
Nafion/PVA	19.3 ± 0.1	0.33 ± 0.1	0.012	[92]
Nafion/PVA	27.9 ± 0.1	0.45 ± 0.1	0.016	[92]
Nafion/PVA	25.8 ± 0.1	0.58 ± 0.1	0.025	[92]
Nafion/PVA	22.9 ± 0.1	0.57 ± 0.1	0100	[92]
Nafion®	227.0 ± 0.1	0.93 ± 0.1	0.027	[92]
Nafion®	27.0 ± 0.1	0.93 ± 0.1	0.034	[92]
Nafion 117	21.5 ± 0.1	0.91 ± 0.1	0.09	[92]

range of 25 °C to 80 °C. Notably, the conductivities tended to increase nearly linearly with the increase in filler content up to 10 wt% and temperature. The conductivity values are dependent on various factors related to GO, such as its aspect ratio, sulfonation or functionalization, and loading amount [93]. The sulfonation process may also induce more interactions between GO and the polymer matrix as sulfonated functionalities anchored on the surface of GO create a strong interaction, such as hydrogen bonding with the OH group in the PVA–PVP blend, compared with –COOH/OH of unmodified GO [94].

The possible proton conduction mechanism in PPMG composite electrolyte is illustrated in Scheme 1. The conductivity results showed that by incorporating SGO nanoparticles, the proton conductivity was considerably improved. This phenomenon can be attributed to the interaction between –sulfonic acid (SO_3H) and hydroxyl (–OH) moieties of the nanofiller and H_2O molecules, which results in more water uptake. In addition, SGO has a high surface area and large number of SO_3H functionalities; hence, it can grasp more H_2O molecules and transport protons more easily via the vehicle mechanism, thus enhancing proton conductivity [95]. Similar results were reported by Jang et al. [96] "integration of SGO into polymer matrix dramatically raises the water absorption and consequently proton conductivity."

The blending of PVP with PVA can increase the amorphous phase and decrease the crystallinity of the resultant composite membrane, which facilitates ionic movement, another factor contributing to enhanced proton transfer. The proton conductivities of PPMG composite membranes are also associated with the hydrophilic characteristics of PVA, which results in increased water retention and a strong hydrogen connection between water and PVP [97]. PVP has significant hydrophilicity and could develop strong hydrogen bonding with water because of the high polarity of its –N–C=O group, which leads to increased water retention and improved proton conduction in the resultant composite membranes [32].

The higher ionic conductivity at higher filler content (SGO) is linked with the availability of SO_3^- groups at the surface of PEMs. This increased concentration of ionizable groups facilitates ionic transfer through the Grotthuss mechanism, wherein protons (H_3O_+) move from one molecule to another, often aided by SO_3^- groups, thus enabling efficient proton transport across the membrane [98].

The highest proton conductivity value of 0.060 S/cm is obtained with a polymer electrolyte membrane having 6 wt% SGO content. Afterward, the value of proton conductivity tends to decrease with the further increase in SGO content, which can be attributed to the fact that nanomaterials with large surface areas are particularly unstable and try to interact with each other, leading to the formation of aggregates that affects their specific surface area and reduces
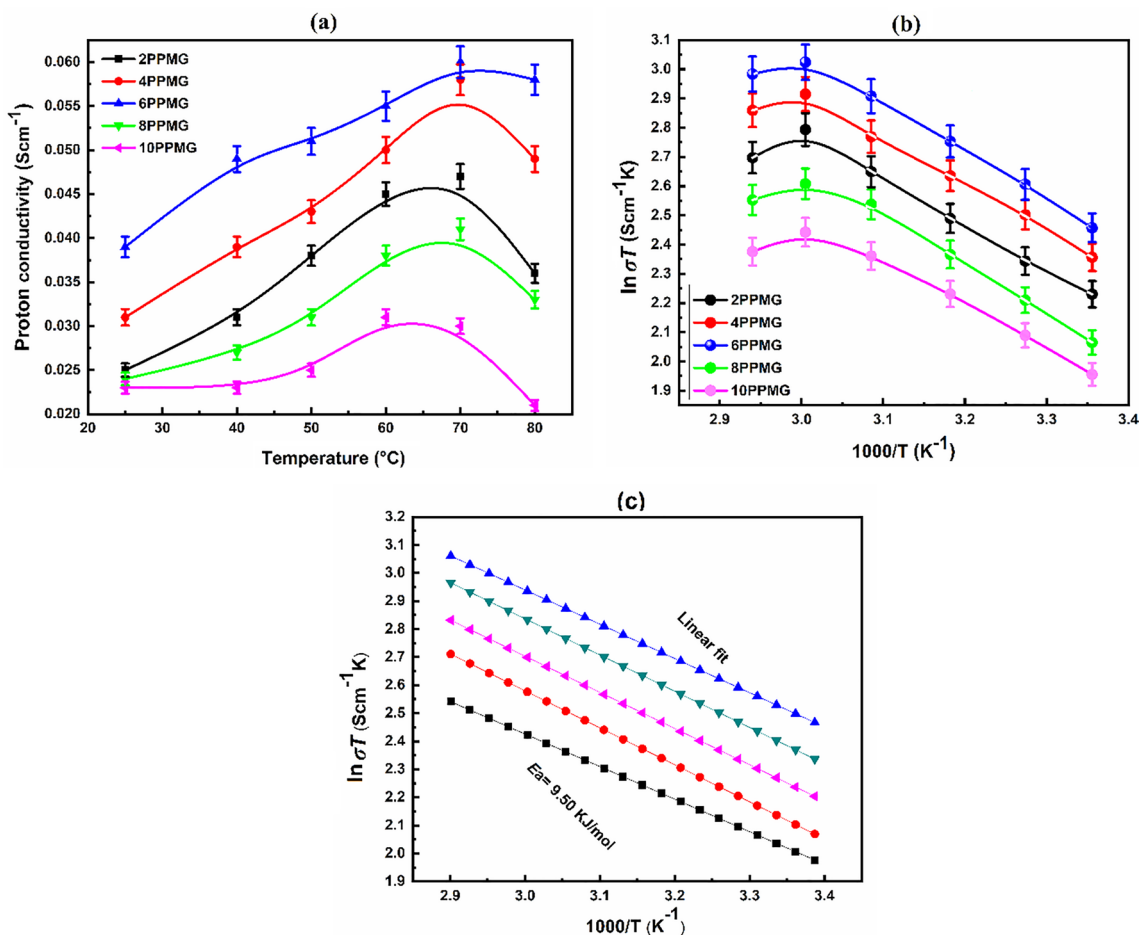
Fig. 7 a Proton conductivity of the prepared composite membranes at different temperatures, **b** Arrhenius plot, and **c** linear fit of the prepared composite membranes

their water uptake and proton transfer capability. In addition, aggregated SGO nanoparticles could inhibit the movement of the polymer chain, which would impede the passage of ions [99, 100]. The variation in conductivity of the prepared composite membrane with the increase in temperature is attributed to the enhancement of the segmental motion of the polymer chain, which, in turn, produces more free volume [32]. These segmental motions facilitate the transmission of ions by providing a passage for the transfer of protons or by hopping from one location to another. Consequently, the segmental motion of the polymer chain facilitates simple ionic mobility. In other words, the segmental motion of the polymer chain aids in facilitating smooth ionic motion. The maximum proton conductivity was observed at 70 °C and tended to decrease at temperatures higher than 70 °C, which can be attributed to the evaporation of membrane water [101] (Table 3).

Table 3 Proton conductivities of PPMG composite membranes at different temperatures

Temperature (°C)	Membranes				
	2PPMG	4PPMG	6PPMG	8PPMG	10PPMG
25	0.025	0.031	0.039	0.024	0.023
40	0.031	0.039	0.049	0.027	0.023
50	0.038	0.043	0.051	0.031	0.025
60	0.045	0.050	0.055	0.038	0.031
70	0.047	0.058	0.060	0.041	0.030
80	0.036	0.049	0.058	0.033	0.020

The activation energy, representing the minimum energy necessary for proton transfer, is calculated for each membrane using Eq. (5):

$$\text{In } \sigma = \frac{E_a}{RT} \tag{5}$$

where σ is the proton conductivity (S/cm), E_a is the activation energy (kJ/mol), R is the universal gas constant ($=8.314$ J/(mol K), and T is the absolute temperature (K).

The activation energies for 2PPMG, 4PPMG, 6PPMG, 8PPMG, and 10PPMG were 9.50, 11.15, 10.32, 10.93, and 10.90 kJ/mol, respectively, as shown in Fig. 7b, c. These activation energies of PPMG composite PEMs, even with small SGO content, are close to that of pristine Nafion® PEMs (9 kJ/mol).

The higher value of activation energy with higher filler content is related to the bound water to free water ratios. The polymer matrix has a higher ratio, although the occurrence of free water facilitates proton transport, but it evaporates faster than bound water. The introduction of filler to the polymer matrix increases the ratio of bound water because of the strong hydrogen bonds between filler and polymer [102], which, in turn, enhances the ionic conductivity of the PPMG membrane compared with virgin polymer matrix [103]. Thus, in SGO-reinforced PEM membranes, the proton conductivity increases with the specific increase in temperature because of their good water retention capacity. Hence, the hybrid membranes exhibit significant advantages at higher temperatures. The proton conductivities of the prepared PPMG composite PEMs are compared with those of other membranes reported in Table 4.

Table 4 Comparison of the proton conductivities of fuel cell composite membranes reported in the literature

| Membranes	Proton conductivity (σ) (S/cm) (25 °C)	References
CS/5 wt% Sulfonated GO	0.0033	[75]
Chitosan (CS)	0.0013	[104]
CS/5 wt% Graphene Oxide	0.0019	[104]
Chitosan/10 wt% sulfonated	0.0022	[104]
CS/SCS/5GO	0.0028	[104]
Cross-linkedSPEEK/	0.0090	[92]
SPVA/SCS blend (90:10) ratio	0.00386	[104]
SPEEK membrane/ (BPO4)	0.00335	[105]
Nafion/PVA	0.012	[92]
Nafion/PVA	0.016	[92]
Nafion/PVA	0.012	[92]
Nafion/PVA	0.025	[92]
Nafion®	0.027	[92]
Nafion/PVA	0100	[92]
Nafion®	0.034	[92]
Nafion 117	0.090	[92]
2PPPMG	0.030	Present work
4PPMG	0.031	Present work
6PPMG	0.039	Present work
8PPMg	0.024	Present work
10PPMG	0.023	Present work

FC Performance

A single-cell performance test for PEMFCs using PPMG composite membranes is conducted with H_2 (fuel) and O_2 (oxygen) at 25 °C and 70 °C (Fig. 8a. The results showed that the increase in temperature leads to the enhancement of the FC performance. Temperature is the pivotal factor that boosts the electrochemical characteristics of FCs [83]. With the increase in temperature from 25 °C to 70 °C, a notable shift in peak power density, i.e., 14.9–35.60 mW/cm^2, was observed. The current density was enhanced from 53.0 mA/cm^2 to 219 mA/cm^2 with 6PPMG (6 wt% SGO content).

For the durability test, the most conductive membrane, i.e., 6PPMG, was chosen and tested at a temperature of 70 °C, with H_2 supplied at a rate of 46 cm^3/s and O_2 supplied at a rate of 100 cm^3/s. The test was conducted for 1,000 h with a constant voltage of 0.3 V. Initially, the current density value obtained was 97.7 mA/cm^2, which continuously decreased during the 1000 h operating time, as shown in Fig. 8b. The final current density of 89.6 mA/cm^2 was reached after 1000 h of continuous operation. The decrease in cell performance can be attributed to the decrease in electrolyte efficiency after continuous operation at 70 °C [106]. The durability results showed that the newly prepared PPMG composite membrane with 6 wt% SGO content exhibited high efficiency and sustainable performance during the 1000 h operating time.

The durability of the pristine PVA–PVP blend membrane and the maximum OCV value of the pristine PV and PVP blend membrane were also analyzed, as depicted in Fig. 8c. The high durability of composite PEM is attributed to the presence of stable SGO filler, which strengthens the resultant composite PEM.

Vinothkannan et al. [43] prepared functionalized carbon nanotube-based PEMs and obtained good results in terms of durability and performance because of the presence of an inorganic filler. A similar study was reported by Kim et al. [107], where PEMs with enhanced electrochemical performance were prepared using phenylsulfonic acid-functionalized and unzipped graphite nanofiber (SO_3H-UGNF) and SPEEK matrix.

To examine the permanent degradation of PEMFCs, a single-cell performance test of 6PPMG was conducted after the durability test. The results are shown in Fig. 8d. The change in the current and power densities of the 6PPMG before and after the durability test was observed. Before the durability test, the current density was 219 mA/cm^2, which was reduced to 189 mA/cm^2. Meanwhile, the maximum power density was reduced to 28.83 W/cm^2. The power loss depended on the current loss. The decrease in cell performance was attributed to the decrease in electrolyte efficiency [108].
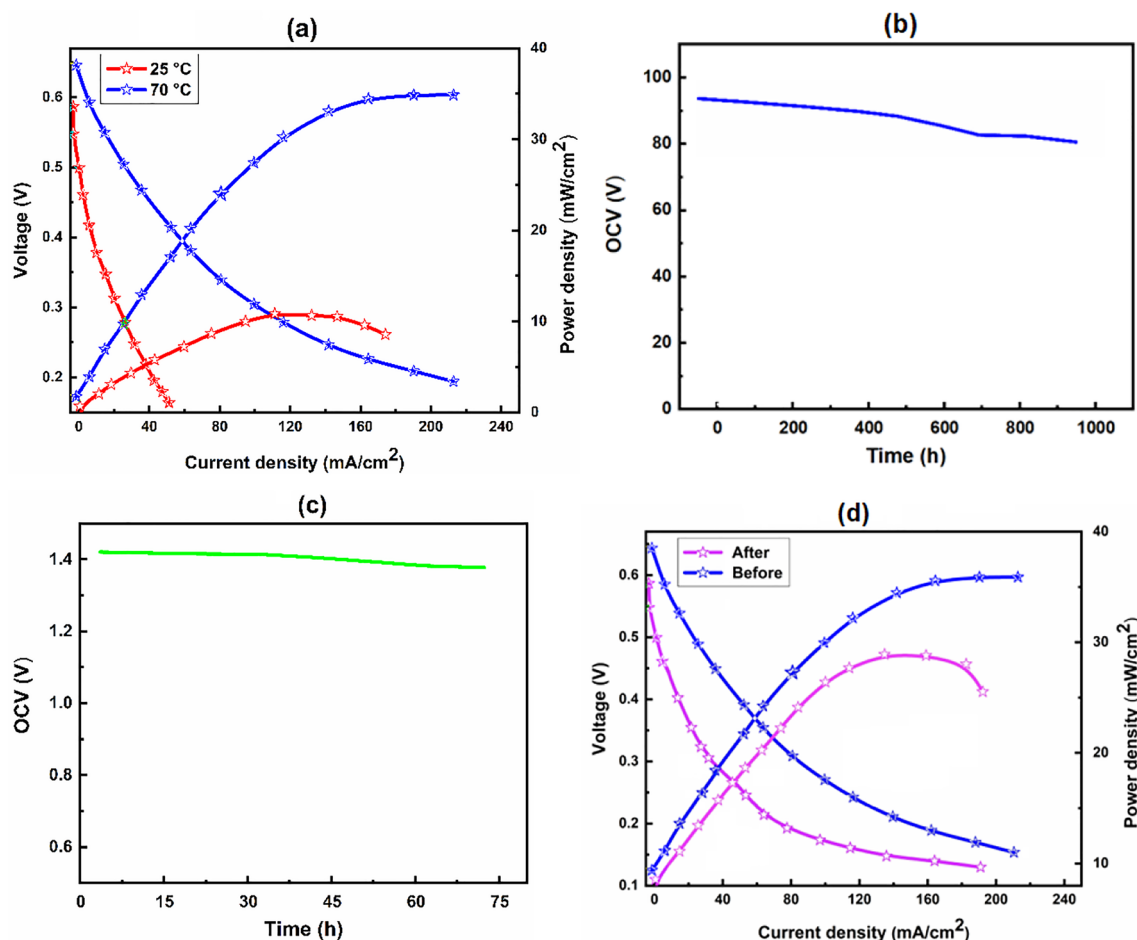
Fig. 8 **a** Single-cell performance test of the prepared composite membranes at 25 °C and 70 °C; durability test of **b** the prepared composite membrane, **c** the prepared pristine PEM; **d** Fuel cell performance before and after the durability test

The results showed that PEMFCs with PPMG composite membranes exhibited good electrochemical performance under ambient conditions. Importantly, the prepared PPMG composite membrane is a more cost-effective alternative to the expensive perfluorosulfonated Nafion® 117 membrane.

Summary and Conclusion

The prepared PPMG electrolytes composed of sulfonated filler and PVA–PVP matrix were fabricated by the solution casting procedure. Before its introduction to the PVA–PVP blend, GO was functionalized using a sulfonating agent to incorporate functional groups and achieve maximum dispersion. The proton conductivity, water uptake, swelling percentage, and CEC of the prepared PEMs with SGO content ranging from 2 wt% to 10 wt% were investigated. The proton conductivities of the PPMG samples were analyzed by the increasing filler content and temperature. The

conductivity values ranged from 0.025 S/cm to 0.060 S/cm. The functionalized SGO filler containing $-SO_3H$ as the ionic source increased the CEC and ionic conductivity of the prepared composite membrane. The formation of strong hydrogen bonds between SO_3H groups and organic polymer chains enabled hydrophilic–hydrophobic phase separation and provided a suitable system for proton conduction. The presence of SGO results in lower water uptake and swelling percentage because of improvement in the dimensional stability of the prepared composite membranes. The performance test of the PEMFC utilizing H_2 and O_2 feeds at temperatures of 25 °C and 70 °C yielded satisfactory results. This study underscores the significant potential of PPMG composite membranes for utilization in PEMFCs.

Declarations

Conflict of interest All authors declare that there are no competing interests.

References

1. Soudagar MEM, Shelare S, Marghade D et al (2024) Optimizing IC engine efficiency: a comprehensive review on biodiesel, nanofluid, and the role of artificial intelligence and machine learning. Energy Convers Manag 307:118337

2. Pramuanjaroenkij A, Kakaç S (2023) The fuel cell electric vehicles: the highlight review. Int J Hydrog Energy 48(25):9401–9425

3. Yuan HB, Zou WJ, Jung S et al (2022) Optimized rule-based energy management for a polymer electrolyte membrane fuel cell/battery hybrid power system using a genetic algorithm. Int J Hydrog Energy 47(12):7932–7948

4. Altaf F, Batool R, Gill R et al (2021) Synthesis and electrochemical investigations of ABPBI grafted montmorillonite based polymer electrolyte membranes for PEMFC applications. Renew Energy 164:709–728

5. Altaf F, Gill R, Batool R et al (2020) Synthesis and applicability study of novel poly(dopamine)-modified carbon nanotubes based polymer electrolyte membranes for direct methanol fuel cell. J Environ Chem Eng 8(5):104118

6. Ryu T, Sutradhar SC, Ahmed F et al (2017) Synthesis and characterization of sulfonated mutiphenyl conjugated polyimide for PEMFC. J Ind Eng Chem 49:99–104

7. Martos AM, Biasizzo M, Trotta F et al (2017) Synthesis and characterization of sulfonated PEEK-WC-PES copolymers for fuel cell proton exchange membrane application. Eur Polym J 93:390–402

8. Blal M, Benatiallah A, NeÇaibia A et al (2019) Contribution and investigation to compare models parameters of (PEMFC), comprehensives review of fuel cell models and their degradation. Energy 168:182–199

9. Ferng YM, Su A, Hou J (2014) Parametric investigation to enhance the performance of a PBI-based high-temperature PEMFC. Energy Convers Manag 78:431–437

10. Baroutaji A, Arjunan A, Robinson J et al (2021) PEMFC polygeneration systems: developments, merits, and challenges. Sustainability 13(21):11696

11. Abbasi NM, Hameed MU, Nasim N et al (2022) Plasmonic nano silver: an efficient colorimetric sensor for the selective detection of Hg^{2+} ions in real samples. Coatings 12(6):763

12. Lim K, Vaz N, Lee J et al (2020) Advantages and disadvantages of various cathode flow field designs for a polymer electrolyte membrane fuel cell. Int J Heat Mass Transf 163:120497

13. Ahmed S, Jiang X, Wang C et al (2021) An insightful picture of nonlinear photonics in 2D materials and their applications: recent advances and future prospects. Adv Opt Mater 9(11):2001671

14. Sharma A, Đelević L, Herkendell K (2024) Next-generation proton-exchange membranes in microbial fuel cells: overcoming nafion's limitations. Energy Tech 2301346

15. Ali A, Al-Othman A, Tawalbeh M (2024) Polymer membranes: general principles and applications in fuel cells. Polymer Membranes: Increasing Energy Efficiency 115–138

16. Thanganathan U, Nogami M (2015) Investigations on effects of the incorporation of various ionic liquids on PVA based hybrid membranes for proton exchange membrane fuel cells. Int J Hydrog Energy 40(4):1935–1944

17. Khalid F, Roy AS, Parveen A et al (2024) Fabrication of the cross-linked PVA/TiO_2/C nanocomposite membrane for alkaline direct methanol fuel cells. Mater Sci Eng B 299:116929

18. Altaf F, Batool R, Gill R et al (2019) Synthesis and characterization of Co-doped ceria-based electrolyte material for low temperature solid oxide fuel cell. Ceram Int 45(8):10330–10333

19. Maiti J, Kakati N, Lee SH et al (2012) Where do poly(vinyl alcohol) based membranes stand in relation to Nafion® for direct methanol fuel cell applications? J Power Sources 216:48–66

20. Kumar P, Das P (2023) Development of sulfonated poly(vinyl alcohol)/MoS_2-based robust composite proton exchange membranes with higher selectivity. ACS Appl Polym Mater 5(10):8459–8473

21. Yang CC, Chien WC, Li YJ (2010) Direct methanol fuel cell based on poly(vinyl alcohol)/titanium oxide nanotubes/poly(styrene sulfonic acid) (PVA/nt-TiO_2/PSSA) composite polymer membrane. J Power Sources 195(11):3407–3415

22. Kim DJ, Jo MJ, Nam SY (2015) A review of polymer–nanocomposite electrolyte membranes for fuel cell application. J Ind Eng Chem 21:36–52

23. Shen J, Xi J, Zhu W et al (2006) A nanocomposite proton exchange membrane based on PVDF, poly(2-acrylamido-2-methyl propylene sulfonic acid), and nano-Al_2O_3 for direct methanol fuel cells. J Power Sources 159(2):894–899

24. Beydaghi H, Javanbakht M, Salar Amoli H et al (2011) Synthesis and characterization of new proton conducting hybrid membranes for PEM fuel cells based on poly(vinyl alcohol) and nanoporous silica containing phenyl sulfonic acid. Int J Hydrog Energy 36(20):13310–13316

25. Sachan VK, Devi A, Katiyar RS et al (2014) Proton transport properties of sulphanilic acid tethered poly(methyl vinyl ether-alt-maleic anhydride)-PVA blend membranes. Eur Polym J 56:45–58

26. Helen M, Viswanathan B, Murthy S (2007) Synthesis and characterization of composite membranes based on α-zirconium phosphate and silicotungstic acid. J Membr Sci 292(1–2):98–105

27. Yang CC, Chiu SJ, Kuo SC (2011) Preparation of poly(vinyl alcohol)/montmorillonite/poly(styrene sulfonic acid) composite membranes for hydrogen–oxygen polymer electrolyte fuel cells. Curr Appl Phys 11(1):S229–S237

28. Yu B, Xu X, Cong H et al (2016) The fabrication and application of carbon nanotube films. Curr Org Chem 20(9):984–993

29. Huang A, Dong C, Gao Y et al (2024) Supramolecular complexation of metal oxide clusters in PVDF-PVP blends for large scale fabrication of proton exchange membranes for fuel cells. Polymer 299:126951

30. Lu S, Xiu R, Xu X et al (2014) Polytetrafluoroethylene (PTFE) reinforced poly(ethersulphone)–poly(vinyl pyrrolidone) composite membrane for high temperature proton exchange membrane fuel cells. J Membr Sci 464:1–7

31. Guo Z, Xiu R, Lu S et al (2015) Submicro-pore containing poly(ether sulfones)/polyvinylpyrrolidone membranes for high-temperature fuel cell applications. J Mater Chem A 3(16):8847–8854

32. Attaran AM, Javanbakht M, Hooshyari K et al (2015) New proton conducting nanocomposite membranes based on poly vinyl alcohol/poly vinyl pyrrolidone/$BaZrO_3$ for proton exchange membrane fuel cells. Solid State Ion 269:98–105

33. Kausar A (2020) A review of fundamental principles and applications of polymer nanocomposites filled with both nanoclay and nano-sized carbon allotropes–graphene and carbon nanotubes. J Plast Film Sheeting 36(2):209–228

34. Eggeler YM, Chan KC et al (2023) A review on 3D architected pyrolytic carbon produced by additive micro/nanomanufacturing. Adv Funct Mater 34:2302068

35. Hussain S, Maktedar SS (2023) Structural, functional and mechanical performance of advanced graphene-based composite hydrogels. Results Chem 6:101029

36. Liu WD, Yu Y, Dargusch M et al (2021) Carbon allotrope hybrids advance thermoelectric development and applications. Renew sustain Energy Rev 141:110800

37. Maiti TK, Dixit P, Singh J et al (2023) A novel strategy toward the advancement of proton exchange membranes through the incorporation of propylsulfonic acid-functionalized graphene oxide in crosslinked acid-base polymer blends. Int J Hydrog Energy 48(4):1482–1500

38. Liu Y, Mao X, Wu H et al (2022) Sulfonated lignin intercalated graphene oxide membranes for efficient proton conduction. J Membr Sci 644:120126

39. Zhang L, Liu Z, Yang C et al (2022) Conduction mechanism in graphene oxide membranes with varied water content: from proton hopping dominant to ion diffusion dominant. ACS Nano 16(9):13771–13782

40. Pandey RP, Shukla G, Manohar M et al (2017) Graphene oxide based nanohybrid proton exchange membranes for fuel cell applications: an overview. Adv Colloid Interface Sci 240:15–30

41. Zeng X, Zhu BB, Qiu W et al (2022) A review of the preparation and applications of wrinkled graphene oxide. N Carbon Mater 37(2):290–302

42. Heo Y, Im H, Kim J (2013) The effect of sulfonated graphene oxide on sulfonated poly (ether ether ketone) membrane for direct methanol fuel cells. J Membr Sci 425–426:11–22

43. Hariprasad R, Vinothkannan M, Kim AR et al (2020) SPVdF-HFP/SGO nanohybrid proton exchange membrane for the applications of direct methanol fuel cells. J Dispers Sci Technol 42(1):33–45

44. Beydaghi H, Javanbakht M, Bagheri A et al (2015) Novel nanocomposite membranes based on blended sulfonated poly(ether ether ketone)/poly(vinyl alcohol) containing sulfonated graphene oxide/Fe$_3$O$_4$ nanosheets for DMFC applications. RSC Adv 5(90):74054–74064

45. Chien HC, Tsai LD, Huang CP et al (2013) Sulfonated graphene oxide/Nafion composite membranes for high-performance direct methanol fuel cells. Int J Hydrog Energy 38(31):13792–13801

46. He Y, Wang J, Zhang H et al (2014) Polydopamine-modified graphene oxide nanocomposite membrane for proton exchange membrane fuel cell under anhydrous conditions. J Mater Chem A 2(25):9548

47. Pandey RP, Shahi VK (2015) Sulphonated imidized graphene oxide (SIGO) based polymer electrolyte membrane for improved water retention, stability and proton conductivity. J Power Sources 299:104–113

48. Kumar R, Mamlouk M, Scott K (2014) Sulfonated polyether ether ketone–sulfonated graphene oxide composite membranes for polymer electrolyte fuel cells. RSC Adv 4(2):617–623

49. Méndez-Lozano N, Pérez-Reynoso F, González-Gutiérrez C (2022) Eco-friendly approach for graphene oxide synthesis by modified hummers method. Materials 15(20):7228

50. Altaf F, Batool R, Gill R et al (2020) Novel N-p-carboxy benzyl chitosan/poly (vinyl alcohol/functionalized zeolite mixed matrix membranes for DMFC applications. Carbohydr Polym 237:116111

51. Altaf F, Gill R, Batool R et al (2019) Proton conductivity and methanol permeability study of polymer electrolyte membranes with range of functionalized clay content for fuel cell application. Eur Polym J 110:155–167

52. Surekha G, Venkata Krishnaiah K, Ravi N et al (2020) FTIR, Raman and XRD analysis of graphene oxide films prepared by modified Hummers method. J Phys: Conf Ser 1495(1):012012

53. Zahid M, Khalid T, Ahmad Rehan Z et al (2021) Fabrication and characterization of sulfonated graphene oxide (SGO) doped PVDF nanocomposite membranes with improved anti-biofouling performance. Membranes 11(10):749

54. Basha IK, Abd El-Monaem EM, Khalifa RE et al (2022) Sulfonated graphene oxide impregnated cellulose acetate floated beads for adsorption of methylene blue dye: optimization using response surface methodology. Sci Rep 12(1):9339

55. Basak P, Dey S, Ghosh P (2020) Sulfonated graphene-oxide as metal-free efficient carbocatalyst for the synthesis of 3-methyl-4-(hetero)arylmethylene isoxazole-5(4H)-ones and substituted pyrazole. ChemistrySelect 5(2):626–636

56. Arenas-Blanco BA, Pérez-Rodríguez EM, Hernández RC et al (2021) Sulfonated graphene oxide nanofluid: potential applications for enhanced oil recovery. Energy Fuels 35(24):20071–20078

57. Franca T, Goncalves D, Cena C (2022) ATR-FTIR spectroscopy combined with machine learning for classification of PVA/PVP blends in low concentration. Vib Spectrosc 120:103378

58. Sadiq M, Raza MMH, Murtaza T et al (2021) Sodium ion-conducting polyvinylpyrrolidone (PVP)/polyvinyl alcohol (PVA) blend electrolyte films. J Electron Mater 50(2):403–418

59. Mireles LK, Wu MR, Saadeh N et al (2020) Physicochemical characterization of polyvinyl pyrrolidone: a tale of two polyvinyl pyrrolidones. ACS Omega 5(47):30461–30467

60. Beygmohammdi F, Nourizadeh Kazerouni H, Jafarzadeh Y et al (2020) Preparation and characterization of PVDF/PVP-GO membranes to be used in MBR system. Chem Eng Res Des 154:232–240

61. Fan X, Ou Y, Yang H et al (2024) Composite proton exchange membrane for fuel cells based on chitosan modified by acid-base amphoteric nanoparticlesInt. J Biol Macromol 254:127796

62. Zerriouh A, Deghiche A, Bououden W et al (2023) A computational and experimental investigation of TEOS-treated graphene oxide-PVA interaction: molecular dynamics simulation and COSMO-RS insights. J Mol Liq 382:121914

63. Nakagawa K, Araya S, Ushio K et al (2021) Controlling interlayer spacing and organic solvent permeation in laminar graphene oxide membranes modified with crosslinker. Sep Purif Technol 276:119279

64. Yusoff YN, Loh KS, Wong WY et al (2020) Sulfonated graphene oxide as an inorganic filler in promoting the properties of a polybenzimidazole membrane as a high temperature proton exchange membrane. Int J Hydrog Energy 45(51):27510–27526

65. Ahmed S, Rui W, Altaf F et al (2022) Nonlinear optical absorption and ultrafast carrier's dynamics of ZrTe$_2$ by transient absorption (TA) spectrometer. Opt Mater 132:112730

66. Meera K, Ramesan MT (2023) A review on the influence of various metal oxide nanoparticles on structural, morphological, optical, thermal and electrical properties of PVA/PVP blends. J Thermoplast Compos Mater 1–22

67. Fu X, Lin J, Liang Z et al (2023) Graphene oxide as a promising nanofiller for polymer composite. Surf Interfaces 37:102747

68. Khan J, Naseem I, Bibi S et al (2022) Green synthesis of silver nanoparticles (Ag-NPs) using Debregeasia salicifolia for biological applications. Materials 16(1):129

69. Khilji MUN, Nahyoon NA, Mehdi M et al (2023) Synthesis of novel visible light driven MgO@GO nanocomposite photocatalyst for degradation of Rhodamine 6G. Opt Mater 135:113260

70. Wang G, Yang S, Kang NY et al (2023) Sulfonated graphene oxide doped sulfonated polybenzothiazoles for proton exchange membrane fuel cells. J Membr Sci 668:121239

71. Majumdar R, Mishra U, Mahata N et al (2023) Preparation, characterization, and performance evaluation of composite films of polyvinyl alcohol/cellulose nanofiber extracted from Imperata cylindrica. Chemosphere 337:139370

72. Jiang ZJ, Jiang Z, Tian X et al (2017) Sulfonated holey graphene oxide (SHGO) filled sulfonated poly(ether ether ketone) membrane: the role of holes in the SHGO in improving its performance as proton exchange membrane for direct methanol fuel cells. ACS Appl Mater Interfaces 9(23):20046–20056

73. Shan K, Yi ZZ, Yin XT et al (2020) Mixed conductivity evaluation and sensing characteristics of limiting current oxygen sensors. Surf Interfaces 21:100762

74. Sahu AK, Ketpang K, Shanmugam S et al (2016) Sulfonated graphene–nafion composite membranes for polymer electrolyte fuel cells operating under reduced relative humidity. J Phys Chem C 120(29):15855–15866

75. Shirdast A, Sharif A, Abdollahi M (2016) Effect of the incorporation of sulfonated chitosan/sulfonated graphene oxide on the proton conductivity of chitosan membranes. J Power Sources 306:541–551

76. Ahmed S, Rui W, Altaf F et al (2022) Ultrafast studies of $ZrTe_3$ by transient absorption spectrometer. Materials 15(15):5420

77. Yan XB, Zhao Y, Cao G et al (2023) 2D organic materials: status and challenges. Adva Sci 10(7):2203889

78. Abd El-Kader MFH, Elabbasy MT, Ahmed MK et al (2021) Structural, morphological features, and antibacterial behavior of PVA/PVP polymeric blends doped with silver nanoparticles via pulsed laser ablation. J Mater Res Technol 13:291–300

79. Modau L, Sigwadi R, Mokrani T et al (2023) Chitosan membranes for direct methanol fuel cell applications. Membranes 13(10):838

80. Zucconi A, Hack J, Stocker R et al (2024) Challenges and opportunities for characterisation of high-temperature polymer electrolyte membrane fuel cells: a review. J Mater Chem A 12(14):8014–8064

81. Vatanpour V, Teber OO, Mehrabi M et al (2023) Polyvinyl alcohol-based separation membranes: a comprehensive review on fabrication techniques, applications and future prospective. Mater Today Chem 28:101381

82. Liu F, Cao Y, Zhang Y et al (2023) Preparation and characterization of N-isopropyl acrylamide grafted polyvinyl alcohol and chitosan blend films with hydrophobic and antibacterial properties. React Funct Polym 188:105604

83. Liu D, Peng J, Li Z et al (2018) Improvement in the mechanical properties, proton conductivity, and methanol resistance of highly branched sulfonated poly(arylene ether)/graphene oxide grafted with flexible alkylsulfonated side chains nanocomposite membranes. J Power Sources 378:451–459

84. Wang B, Ling Z, Li N et al (2023) Graphene oxide-intercalated montmorillonite layered stack incorporated into poly(2, 5-benzimidazole) for preparing wide-temperature proton exchange membranes. ACS Appl Nano Mater 6(21):20355–20366

85. Sonker AK, Rathore K, Nagarale RK et al (2018) Crosslinking of polyvinyl alcohol (PVA) and effect of crosslinker shape (aliphatic and aromatic) thereof. J Polym Environ 26(5):1782–1794

86. El Sayed MM (2023) Production of polymer hydrogel composites and their applications. J Polym Environ 31(7):2855–2879

87. Oroujzadeh M, Ali Nikouei M, Mehdipour-Ataei S et al (2022) Materials selection for choosing the best composite blend polymeric membrane for hydrogen/oxygen proton exchange membrane fuel cell. J Power Sources 538:231566

88. Qu E, Hao X, Xiao M et al (2022) Proton exchange membranes for high temperature proton exchange membrane fuel cells: challenges and perspectives. J Power Sources 533:231386

89. Ranjani M, Pannipara M, Al-Sehemi AG et al (2019) Chitosan/sulfonated graphene oxide/silica nanocomposite membranes for direct methanol fuel cells. Solid State Ion 338:153–160

90. Mondal S, Papiya F, Ash SN et al (2021) Composite membrane of sulfonated polybenzimidazole and sulfonated graphene oxide for potential application in microbial fuel cell. J Environ Chem Eng 9(1):104945

91. Pagliero M, Comite A, Costa C (2024) Mixed matrix and nanocomposite membranes. polymeric membrane formation by phase inversion. Elsevier, Amsterdam, pp 225–266

92. Mollá S, Compañ V (2011) Performance of composite Nafion/PVA membranes for direct methanol fuel cells. J Power Sources 196(5):2699–2708

93. Suhag S, Kumar P, Mandal JR et al (2024) Functionalized graphene oxide-modified sulfonated poly (2, 6-dimethyl-1, 4-phenylene oxide) based thermal-resistance anti-fouling bi-functional cation exchange membrane for electrodialytic desalination. Desalination 578:117454

94. Ng WW, Thiam HS, Pang YL et al (2023) Self-sustainable, self-healable sulfonated graphene oxide incorporated nafion/poly (vinyl alcohol) proton exchange membrane for direct methanol fuel cell applications. J Environ Chem Eng 11(6):111151

95. Li P, He B, Li X et al (2023) Chitosan-linked dual-sulfonate COF nanosheet proton exchange membrane with high robustness and conductivity. Small 19(35):2302060

96. Jang HR, Vinothkannan M, Kim AR et al (2018) Constructing proton-conducting channels within sulfonated(poly arylene ether ketone) using sulfonated graphene oxide: a nano-hybrid membrane for proton exchange membrane fuel cells. Bull Korean Chem Soc 39(6):715–721

97. Maarouf S, Tazi B, Guenoun F (2017) Preparation and characterization of new composite membranes containing polyvinylpyrrolidone, polyvinyl alcohol, sulfosuccinic acid, silicotungstic acid and silica for direct methanol fuel cell applications. J Mater Env Sci 8(8):2870–2876

98. Naseem K, Zhang J, Fayyaz A et al (2024) Enhanced generation of hydrogen through hydrolysis of biochar-coupled magnesium: analysis of the performance of biochar-support and the effect of metallic coating on biochar. J Environ Chem Eng 12(1):111770

99. Salarizadeh P, Javanbakht M, Pourmahdian S (2017) Enhancing the performance of SPEEK polymer electrolyte membranes using functionalized TiO_2 nanoparticles with proton hopping sites. RSC Adv 7(14):8303–8313

100. Liu Q, Luo Y, Yang S et al (2023) Transfer-free in situ synthesis of high-performance polybenzimidazole grafted graphene oxide-based proton exchange membrane for high-temperature proton exchange membrane fuel cells. J Power Sources 559:232666

101. Zhao J, Song D, Jia J et al (2022) Constructing proton exchange membranes with high and stable proton conductivity at subzero temperature through vacuum assisted flocculation technique. Appl Surf Sci 585:152579

102. Altaf F, Ahmed S, Dastan D et al (2022) Novel sepiolite reinforced emerging composite polymer electrolyte membranes for high-performance direct methanol fuel cells. Mater Today Chem 24:100843

103. Rhim J, Park H, Lee C et al (2004) Crosslinked poly(vinyl alcohol) membranes containing sulfonic acid group: proton and methanol transport through membranes. J Membr Sci 238(1–2):143–151

104. Atkar A, Sridhar S, Deshmukh S et al (2024) Synthesis and characterization of sulfonated chitosan (SCS)/sulfonated polyvinyl alcohol (SPVA) blend membrane for microbial fuel cell application. Mater Sci Eng B 299:116942

105. Yang T (2009) Composite membrane of sulfonated poly(ether ether ketone) and sulfated poly(vinyl alcohol) for use in direct methanol fuel cells. J Membr Sci 342(1–2):221–226

106. Wan J, Wang R, Liu Z et al (2024) Hydrated eutectic electrolyte induced bilayer interphase for high-performance aqueous Zn-ion batteries with 100 ℃ wide-temperature range. Adv Mater 36(11):2310623

107. Kim AR, Vinothkannan M, Ramakrishnan S et al (2022) Enhanced electrochemical performance and long-term durability of composite membranes through a binary interface with sulfonated unzipped graphite nanofibers for polymer electrolyte fuel cells operating under low relative humidity. Appl Surf Sci 593:153407

108. Sakas G, Ibáñez-Rioja A, Pöyhönen S et al (2024) Influence of shunt currents in industrial-scale alkaline water electrolyzer plants. Renew Energy 225:120266
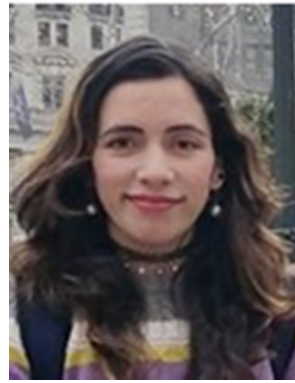
Dr. Faizah Altaf is a Postdoctoral Fellow at Interdisciplinary Research Centre for Hydrogen and Energy Storage (IRC-HES), KFUPM. She completed her PhD degree (2020) in Environmental Chemistry from Fatima Jinnah Women University, Rawalpindi, Pakistan. During her PhD, she focused on "synthesis and electrochemical investigations of polymer-based polymer electrolyte membranes for PEMFC applications." She is currently focusing on polymer-based composite for fuel cell applications, membrane developments for redox flow battery systems and materials designing for CO_2 sequestration applications.

Dr. Shakeel Ahmed completed his PhD degree in 2023 in the field Optical Engineering from Shenzhen University, China. During his PhD, he focused on the "Nonlinear Optical Properties of 2D Materials, using Femtosecond Transient Absorption Spectroscopy. He is currently working on polymer based composite for Fuel cell applications and electrolysis of diamond composites for Optoelectronics Applications.